

# Probing Supersymmetry With Third-Generation Cascade Decays

Michael Graesser<sup>1</sup> and Jessie Shelton<sup>2</sup>

<sup>1</sup>*Theory Division, T-2  
Los Alamos National Laboratory  
Los Alamos, NM 87545*

<sup>2</sup>*Department of Physics  
Rutgers University  
Piscataway, NJ 08854*

## Abstract

The chiral structure of supersymmetric particle couplings involving third generation Standard Model fermions depends on left-right squark and slepton mixings as well as gaugino-higgsino mixings. The shapes and intercorrelations of invariant mass distributions of a first or second generation lepton with bottoms and taus arising from adjacent branches of SUSY cascade decays are shown to be a sensitive probe of this chiral structure. All possible cascade decays that can give rise to such correlations within the MSSM are considered. For bottom-lepton correlations the distinctive structure of the invariant mass distributions distinguishes between decays originating from stop or sbottom squarks through either an intermediate chargino or neutralino. For decay through a chargino the spins of the stop and chargino are established by the form of the distribution. When the bottom charge is signed through soft muon tagging, the structure of the same-sign and opposite-sign invariant mass distributions depends on a set function of left-right and gaugino-higgsino mixings, as well as establishes the spins of all the superpartners in the sequential two-body cascade decay. Tau-lepton and tau-tau invariant mass distributions arising from MSSM cascade decays are likewise systematically considered with particular attention to their dependence on tau polarization. All possible tau-lepton and tau-tau distributions are plotted using a semi-analytic model for hadronic one-prong taus. Algorithms for fitting tau-tau and tau-lepton distributions to data are suggested.

# 1 Introduction

As the LHC prepares to uncover the physics responsible for electroweak symmetry breaking, third-generation fermions present especially interesting possibilities as their large Yukawa couplings make them uniquely sensitive to details of chiral physics at the electroweak scale. Moreover, in the context of SUSY, there are several reasons to anticipate that SUSY signals may be substantially third-generation enriched. The LEP2 bounds on the masses of MSSM Higgs bosons [1] suggest that  $\cos 2\beta \simeq 1$ , to maximize the tree-level contribution to the Higgs mass, favoring moderate or larger  $\tan \beta$ . At large  $\tan \beta$ , the enhanced Yukawa couplings of the  $b$  and  $\tau$  contribute negatively to the running of the sbottom and stau soft masses, so that sbottoms, staus, and stops all tend to be lighter than the other sfermions. Large Yukawas also enhance the coupling of sfermions to higgsinos, thereby increasing the sensitivity of sparticle decays to gaugino-higgsino mixing. In addition, large  $\tan \beta$  can lead to large left-right sbottom and stau mixing, further lowering sbottom and stau masses [2]. Light stops and large sfermion mixing are also motivated by the desire to minimize the tuning in the quantum corrections to the Higgs mass [3]. Light third-generation sfermions lead to a significant enrichment of third-generation final states in the signal [2].

Third-generation fermions have complicated in-detector decays which require more effort to identify and understand. On the other hand, these complicated decays allow for measurement of interesting properties such as polarization (tops, taus) and charge (bottoms) which are inaccessible for the lighter fermions. Exploiting these properties allows for detailed measurement of various aspects of the Lorentz and chiral structure of new physics.

In this paper we consider SUSY cascade decays which produce third-generation fermions in the final state. Our interest here is to survey the space of possibilities. Decades of work on supersymmetry breaking and its mediation to the Standard Model have led to a dizzying variety of predictions for possible sparticle spectra. At the same time, the continuing absence of deviations from the Standard Model predictions gives no hints as to which, if any, of these spectra may be preferred. In this paper we enumerate all possible patterns of invariant mass distributions for  $b$ - $l$ ,  $l$ - $\tau$ , and  $\tau$ - $\tau$  pairs which arise from adjacent legs of on-shell SUSY cascade decays, and demonstrate how the special properties of  $b$ 's and  $\tau$ s can be used to obtain further information about the chiral properties of the MSSM. Our analysis is model-independent insofar as it is independent of the spectrum of superpartner masses; we assume only the existence of on-shell decay modes, the Lorentz structure of the SUSY vertices, and the field content of the MSSM <sup>1</sup>. This type of model-independent

---

<sup>1</sup>We make in addition a few mild theoretical assumptions, namely: we neglect the electron and muon Yukawa couplings; we neglect SUSY flavor-violating processes; we assume lepton flavor universality holds for electrons and muons. It is interesting to explore what happens to the intercorrelations among invariant

analysis has been applied to related cascade decay signals in [5].

Two-step on-shell SUSY cascades can give three different fundamental shapes for invariant mass distributions [6]. Intermediate scalars, as in the decay chains

$$\chi_i^0 \rightarrow l^\pm \tilde{l}^\mp \rightarrow l^\pm l^\mp \chi_j^0 \quad (1)$$

give a triangular distribution for the invariant mass of the two visible standard model fermions,

$$\frac{1}{\Gamma} \frac{d\Gamma}{dx} = 2x. \quad (2)$$

Here we have defined the rescaled variable

$$x \equiv \frac{m_{ff}}{m_{ff,max}}.$$

Intermediate fermions, as in the decay chains

$$\tilde{b}_{L,R} \rightarrow b \chi_i^0 \rightarrow b \tilde{l}_{L,R}, b \tilde{l}_{R,L} \quad (3)$$

yield ‘‘humps’’

$$\frac{1}{\Gamma} \frac{d\Gamma}{dx} = 4x(1 - x^2) \equiv H(x) \quad (4)$$

and ‘‘half-cusps’’

$$\frac{1}{\Gamma} \frac{d\Gamma}{dx} = 4x^3 \equiv C(x) \quad (5)$$

for processes without and with a helicity flip on the intermediate fermion propagator, respectively. These are the only possibilities when the intermediate particle is on-shell and the two Standard Model fermions to be combined together are adjacent in the decay chain [6].

We categorize the  $b$ - $l$  distributions which can arise from adjacent legs of SUSY cascade decays. In the MSSM,  $b$ - $l$  final states can be produced from either the decay of a stop through a chargino or a sbottom through a neutralino to sleptons. The patterns of  $b$ - $l$  invariant mass distributions arising from these cascade decays have a distinctive structure which discriminates between stop and sbottom initial states and establishes the spin and Dirac nature of the chargino. Signing muonically-decaying  $b$ -quarks using the associated soft muon reveals an additional layer of structure which serves to establish the spin and Majorana nature of the neutralino, as well as the relative handedness of the sbottom and the slepton participating in the decay chain. The ability to establish spins using signed (for neutralino decay chains) or unsigned (for chargino decay chains)  $b$ - $l$  distributions are

---

mass distributions from cascade decays when these mild assumptions are relaxed [4], but that is beyond the scope of the present work.

entirely independent of the existence of a production asymmetry favoring squarks over anti-squarks. The shapes and intercorrelations of the  $b$ - $l$  invariant mass distributions are sensitive to both left-right squark mixing and gaugino-higgsino mixing.

We perform a similar categorization of the  $l$ - $\tau$  and  $\tau$ - $\tau$  invariant mass distributions which can be realized in SUSY two-step cascade decays. As with  $b$ - $l$  distributions, the shapes and intercorrelations of  $l$ - $\tau$  and  $\tau$ - $\tau$  distributions are sensitive to both left-right squark mixing and gaugino-higgsino mixing. Invariant mass distributions involving  $\tau$ s are complicated, however, by the missing four-momentum of the neutrino coming from the decay of the  $\tau$ . The observable invariant mass distributions constructed from the  $\tau$ 's visible hadronic daughters differ significantly from the underlying triangle, hump, and half-cusp distributions. Ditau distributions can nevertheless be used to measure superpartner masses with reasonable precision [7, 8]. Using the shape of  $\tau$ - $\tau$  and  $l$ - $\tau$  invariant mass distributions to further establish more detailed properties of the superpartners requires the  $\tau$  visible daughter energy spectrum to be carefully taken into account.

As the distributions of visible daughter energy depend sensitively on the polarization of the parent  $\tau$  [9, 10, 11, 12], the observable  $l$ - $\tau$  and  $\tau$ - $\tau$  invariant mass distributions are likewise dependent on the  $\tau$  polarization. Exploiting the dependence of the visible hadronic daughters on the parent  $\tau$  polarization enables a direct probe of the chiral structure of the  $\tau$  production vertex, opening interesting possibilities both in Higgs physics [11, 12, 13, 14, 15] and in the MSSM [16, 17, 18, 19, 20]. Careful study of  $l$ - $\tau$  and  $\tau$ - $\tau$  invariant mass distributions arising from cascade decays thereby opens the exciting prospect of directly probing the mixings and electroweak quantum numbers of the superpartners participating in the decay [18, 19]. We use a semi-analytic approximation to the visible daughter energy spectra for the hadronic one-prong decay mode, which provides the most sensitive polarimeter for invariant mass distributions. Using these spectra, we plot the possible theoretical  $l$ - $\tau$  and  $\tau$ - $\tau$  distributions that can arise from SUSY cascade decays, and propose algorithms for fitting these distributions to experimental data.

The outline of the paper is as follows. We begin in Section 2 by considering  $b$ - $l$  final states. Section 3 discusses the possible ditau and lepton-tau distributions in the limit of no mixing. In Section 4 we turn on mixing, and discuss fitting algorithms in subsection 4.1. Our conclusions can be found in Section 5, and details of our treatment of  $\tau$  decay can be found in the Appendix.

## 2 $b$ - $\ell$ distributions

$b$ -quarks are useful tools to study SUSY cascade decays. The presence of  $b$ -tags in an event can help serve to separate signal from background, while the ability to sign semimuonic  $b$ 's using the associated muon goes further to help to shed light on the Lorentz properties of the supersymmetric particles, as we will demonstrate. We will study the invariant mass distributions of  $b$ - $\ell$  pairs which arise from adjacent steps in a cascade decay.

SUSY decay chains which yield adjacent  $b$ -quarks and leptons are the decay of sbottoms through a neutralino or stops through a chargino. Sbottom decays through a neutralino,

$$\tilde{b} \rightarrow b\chi_i^0 \rightarrow b\ell\tilde{l}, \quad (6)$$

yield both ‘‘opposite-sign’’ ( $b^{\pm 1/3}\text{-}\ell^{\mp}$ ) and ‘‘same-sign’’ ( $b^{\pm 1/3}\text{-}\ell^{\pm}$ ) final states. In the limit of zero squark and neutralino mixing, these processes (6) contribute either opposite-sign humps and same-sign cusps if the parent sbottom and the final slepton have the same handedness, or opposite-sign cusps and same-sign humps if the parent sbottom and the final slepton have the opposite handedness.. Stop decays through a chargino,

$$\tilde{t} \rightarrow b\chi_i^{\pm} \rightarrow b\ell\tilde{\nu}, \quad (7)$$

contribute to opposite-sign final states only with no contribution in the same-sign channel. In the limit of zero squark and neutralino mixing, the distribution in the opposite-sign channel from the process (7) is a hump.

In general events with the decay chain(s) (6, 7) will also contain additional leptons coming from the subsequent decay of the sleptons, so there is some ambiguity in selecting which lepton to pair with the  $b$  jet. Some possible approaches to minimizing this combinatoric confusion have been discussed in previous studies of the related decay chain  $\tilde{q} \rightarrow q\chi_i^0 \rightarrow q\ell\tilde{l}$  and its UED counterpart [6, 21, 22, 5]. At present we will concentrate on characterizing the theoretical distribution for the correct  $b$ - $l$  pairing, leaving the question of combinatorics to future work.

The possible SUSY  $b$ - $l$  distributions in the limit of no squark or neutralino mixing are summarized in Table 1 <sup>2</sup>. If (e.g.) the decay chain  $\tilde{b}_L^{\pm} \rightarrow b^{\pm}\chi_i^0 \rightarrow b^{\pm}l^{\mp}\tilde{l}_L^{\pm}$  exists in the signal, then (for a standard Majorana neutralino) so must the decay chain  $\tilde{b}_L^{\pm} \rightarrow b^{\pm}\chi_i^0 \rightarrow b^{\pm}l^{\pm}\tilde{l}_L^{\mp}$ . Therefore there must exist both a hump distribution in the opposite-sign channel and a cusp distribution in the same-sign channel, with equal normalizations and endpoints. Since the hump and the half-cusp sum to a triangle, if the opposite-sign and same-sign channels

---

<sup>2</sup>In the name of generality, we remark that interchanging the role of the squark and slepton does not alter the shapes and correlations of the  $b$ - $l$  distributions, so that (e.g.) the decay chain  $\tilde{b}_L^{\pm} \rightarrow b^{\pm}\chi_i^0 \rightarrow b^{\pm}l^{\mp}\tilde{l}_L^{\pm}$  yields the same  $b$ - $l$  invariant mass distribution as the flipped decay chain  $\tilde{l}_L^{\pm} \rightarrow l^{\pm}\chi_i^0 \rightarrow l^{\pm}b^{\mp}\tilde{b}_L^{\pm}$ .

	Hump	Half-Cusp
Opposite-Sign	$\tilde{b}_L^\pm \rightarrow b^\pm \chi_i^0$ $\hookrightarrow b^\pm l^\mp \tilde{l}_L^\pm$	$\tilde{b}_R^\pm \rightarrow b^\pm \chi_i^0$ $\hookrightarrow b^\pm l^\mp \tilde{l}_L^\pm$
	$\tilde{t}_L^\pm \rightarrow b^\mp \chi_i^\pm$ $\hookrightarrow b^\mp l^\pm \tilde{\nu}_L$	
Same-Sign	$\tilde{b}_L^\pm \rightarrow b^\pm \chi_i^0$ $\hookrightarrow b^\pm l^\pm \tilde{l}_L^\mp$	$\tilde{b}_R^\pm \rightarrow b^\pm \chi_i^0$ $\hookrightarrow b^\pm l^\pm \tilde{l}_L^\mp$

Table 1: Possible invariant mass distributions for the  $b$ - $l$  final states. Here by a slight abuse of notation  $\pm$  distinguishes between (s)quark and anti-(s)quark, so that  $b^\pm$  has charge  $\pm 1/3$ . Distributions for final state  $\tilde{l}_R$  are obtained by exchanging hump and half-cusp. Squark right-left mixing is neglected and neutralinos and charginos are taken to be pure gaugino.

cannot be distinguished, then the information about the spin of the neutralino is lost. Thus the ability to sign the  $b$ -jet allows for determination both of the spin of the neutralino and of its Majorana nature.

When the sbottom and the slepton have the same handedness then opposite sign distributions are humps and same-sign distributions are half-cusps; the situation is reversed when the sbottom and the slepton have different handedness. It is possible to obtain spectra which allow all four possible decay chains ( $\tilde{b}_{L,R} \rightarrow b \tilde{l}_{L,R}$  and  $\tilde{b}_{L,R} \rightarrow b \tilde{l}_{R,L}$ ) to be realized simultaneously. This will complicate spin measurements as the sums of the overlapping distributions coming from these processes will tend to wash out the spin correlations. The greater the mass splitting between right- and left-handed squarks and/or sleptons, the more distinct the endpoints of the different distributions will be, and the easier it will be to disentangle the contributions from different processes to the total  $b$ - $l$  distributions. The possibility of making a spin measurement in this channel will also depend on the relative branching fractions into sleptons of different handedness. Consider the case when right- and left-handed sleptons are nearly degenerate. Then the different gauge quantum numbers of the right- and left-handed sleptons will still yield (e.g.)  $\Gamma(\tilde{b}_L \rightarrow b \chi_i^0 \rightarrow b \tilde{l}_L) / \Gamma(\tilde{b}_L \rightarrow b \chi_i^0 \rightarrow b \tilde{l}_R) \neq 1$ . The total  $b$ - $l$  distribution will then retain some spin information.

Stops, on the other hand, contribute only to the opposite-sign channel, so comparison of opposite-sign and same-sign distributions will be an important tool to disentangle possible contributions from stop and sbottom squarks.

When the intermediate chargino is pure gaugino, only decay chains beginning from initial  $\tilde{t}_L$  can contribute to  $b$ - $l$  final states. However, as the lepton Yukawas are negligible, it is also sensible to consider the case where the chargino is nearly pure higgsino but still decays to lepton-slepton pairs as a gaugino. In this case, the  $\tilde{t}_R$  can decay through an up-type higgsino in the decay chain  $\tilde{t}_R^\pm \rightarrow b^\mp \chi_i^\pm \rightarrow b^\mp l^\pm \tilde{\nu}$ , yielding an opposite-sign hump distribution. The  $\tilde{t}_L$  can decay through a down-type higgsino via the decay chain  $\tilde{t}_L^\pm \rightarrow b^\mp \chi_i^\pm \rightarrow b^\mp l^\pm \tilde{\nu}$ , which yields an opposite-sign half-cusp distribution.

In stop decay, the  $b$ -tag alone suffices to establish that the intermediate fermion is Dirac, rather than Majorana, and the additional sign information is not necessary: if the intermediate fermion were Majorana, then summing the distributions for the final states  $\bar{b}l^-$  and  $b l^-$  would give a triangle, while for an intermediate Dirac particle, only one of the helicity states can contribute, leading to a hump distribution (or a half-cusp distribution when the chargino is a down-type higgsino) even when both final states are summed.

This is an example of a general point: it is possible to observe nontrivial (non-triangular) distributions in the absence of sign information, if a symmetry forbids one channel from contributing (as for stop decays through charginos, here, or as for Dirac neutralinos [4]). Nontrivial distributions also can be obtained if the two channels contribute with unequal weights, as is the case when a production asymmetry favors squarks over anti-squarks [6]. However, event-by-event signing of the semimuonic  $b$ 's allows a direct observation of any angular correlations coming from intermediate Majorana neutralinos, independent of any possible production asymmetry.  $b$ -jet signing as a tool to improve spin measurements at the LHC has been mentioned in [23, 24].

We now go on to discuss how this story is modified in the presence of nontrivial squark and neutralino mixing.

## 2.1 $b$ - $l$ distributions with nontrivial squark and neutralino mixing

Left-right sfermion mixing renders the SUSY sfermion-fermion-gaugino vertices less chiral and thereby alters the observable kinematical distributions [25]. Similarly, higgsino interactions proportional to a fermion Yukawa coupling involve the opposite chirality of the fermion relative to gaugino interactions. Sfermion and neutralino mixings, then, have a qualitatively similar effect on the invariant mass distributions. In this section we will detail the sensitivity of difermion invariant mass distributions to both sfermion mixing and neutralino mixing, including both effects simultaneously. While here we concentrate on

$b$ -quarks and  $b$ - $l$  distributions, the same physics will be relevant to lepton-tau and ditau distributions in section 4.

Consider the hump and half-cusp distributions which arise from decay chains with an intermediate fermion. Once mixing is turned on, both helicity states of the intermediate fermion can contribute to a given channel, with relative weights determined by the mixing. The observable same-sign and opposite-sign distributions are then a weighted sum of hump and half-cusp distributions. Define the squark left-right mixing angles through

$$\tilde{q}_1 = \cos \theta_{\tilde{q}} \tilde{q}_R^* + \sin \theta_{\tilde{q}} \tilde{q}_L. \quad (8)$$

(As usual,  $\tilde{q}_1$  is taken to be the lighter of the two squarks. In our conventions  $q_R$  is a left-handed anti-quark, and thus  $\tilde{q}_R$  is an anti-squark.) Define also the unitary matrix  $U$  which diagonalizes the neutralino mass matrix. The sbottom-bottom-neutralino couplings are then governed by the interaction Lagrangian

$$\mathcal{L} = \tilde{b}_1 \left( b_R \chi_i^0 n_{1,i}^R + (\chi_i^0)^\dagger t_L^\dagger n_{1,i}^L \right) + \tilde{b}_2 \left( b_R \chi_i^0 n_{2,i}^R + (\chi_i^0)^\dagger t_L^\dagger n_{2,i}^L \right) + \text{H.c.} \quad (9)$$

with parameters

$$n_{1,i}^R = \sin \theta_{\tilde{b}} \lambda_b U_{di}^* + \cos \theta_{\tilde{b}} \frac{\sqrt{2} g'}{3} U_{Bi}^* \quad (10)$$

$$n_{1,i}^L = \sin \theta_{\tilde{b}} \left( -\frac{g}{\sqrt{2}} U_{iW} + \frac{g'}{3\sqrt{2}} U_{iB} \right) + \cos \theta_{\tilde{b}} \lambda_b U_{di}^* \quad (11)$$

$$n_{2,i}^R = \cos \theta_{\tilde{b}} \lambda_b U_{di}^* - \sin \theta_{\tilde{b}} \frac{\sqrt{2} g'}{3} U_{Bi}^*, \quad (12)$$

$$n_{2,i}^L = \cos \theta_{\tilde{b}} \left( -\frac{g}{\sqrt{2}} U_{iW} + \frac{g'}{3\sqrt{2}} U_{iB} \right) - \sin \theta_{\tilde{b}} \lambda_b U_{di}^* \quad (13)$$

Note that  $n_{1,i}^L \rightarrow 0$ ,  $n_{2,i}^R \rightarrow 0$  as both mixings are turned off, that is, as  $\theta_{\tilde{b}}, U_{di} \rightarrow 0$ , while  $n_{2,i}^L, n_{1,i}^R$  remain finite. The index  $i$  specifies the neutralino mass eigenstate  $i$ , while the indices  $d, B, W$  run over the gauge eigenstates (here down-type higgsino, bino, and wino, respectively). We now define the angles

$$\cos^2 \alpha_{1i} \equiv \frac{|n_{1,i}^R|^2}{|n_{1,i}^R|^2 + |n_{1,i}^L|^2}, \quad \cos^2 \alpha_{2i} \equiv \frac{|n_{2,i}^L|^2}{|n_{2,i}^L|^2 + |n_{2,i}^R|^2}; \quad (14)$$

in the limit of zero mixing,  $\cos \alpha_{1i}$  and  $\cos \alpha_{2i}$  both go to unity. Decays of sbottoms through the neutralino  $\tilde{\chi}_i^0$  will be weighted by these angles. Meanwhile, the stop-bottom-chargino couplings are governed by the interaction Lagrangian

$$\mathcal{L} = \tilde{t}_1 \left( b_R \chi_i^- c_{1,i}^R + (\chi_i^+)^\dagger b_L^\dagger c_{1,i}^L \right) + \tilde{t}_2 \left( b_R \chi_i^- c_{2,i}^R + (\chi_i^+)^\dagger b_L^\dagger c_{2,i}^L \right) + \text{H.c.} \quad (15)$$

with parameters

$$c_{1,i}^L = -\sin\theta_{\tilde{t}}gV_{iW} + \cos\theta_{\tilde{t}}\lambda_tV_{iu} \quad (16)$$

$$c_{1,i}^R = \sin\theta_{\tilde{t}}\lambda_bW_{di}^* \quad (17)$$

$$c_{2,i}^L = -\cos\theta_{\tilde{t}}gV_{iW} - \sin\theta_{\tilde{t}}\lambda_tV_{iu} \quad (18)$$

$$c_{2,i}^R = \cos\theta_{\tilde{t}}\lambda_bW_{di}^*, \quad (19)$$

The unitary matrix  $V$  (not the CKM matrix!) diagonalizes the positively-charged left-handed charginos ( $\tilde{W}^+, \tilde{h}_u^+$ ), and the unitary matrix  $W$  diagonalizes the negatively-charged left-handed charginos ( $\tilde{W}^-, \tilde{h}_d^-$ ). We then define the angles

$$\cos^2\beta_{1i} \equiv \frac{|c_{1,i}^R|^2}{|c_{1,i}^R|^2 + |c_{1,i}^L|^2}, \quad \cos^2\beta_{2i} \equiv \frac{|c_{2,i}^L|^2}{|c_{2,i}^L|^2 + |c_{2,i}^R|^2}, \quad (20)$$

where again  $\cos\beta_{1i}$  and  $\cos\beta_{2i}$  go to unity in the limit of zero mixing. Decays of stops through the chargino  $\tilde{\chi}_i^+$  will be weighted by these angles. Table 2 summarizes the  $b$ -lepton distributions in the presence of mixing; a similar approach to mixing was taken in [5].

Notice that for stop squark decays through charginos, admixture of the cusp distribution depends on a sizable down-type higgsino component of the intermediate chargino. This can be seen as follows. As the lepton Yukawas are negligible, the chargino decay to lepton-sneutrino pairs will occur through its gaugino component. To obtain a half-cusp distribution, the  $b$  must then be right-handed (as its charge is fixed). But as the wino does not couple to the right-handed  $b$ , a half-cusp distribution can only be obtained if the intermediate chargino has a down-type higgsino component, independent of any possible mixing of the stop squarks. The coupling of the higgsino to the  $b_R$  depends on  $\lambda_b$  and is therefore enhanced at large  $\tan\beta$ . In short, if the chargino is taken to have no down-type higgsino component, then stop mixing alone will not alter the observed hump distribution. In this context it is useful to recall that no sign information of the  $b$ -quark is necessary to observe the hump distribution coming from stop decay.

Fitting the observed  $b$ - $\ell$  distributions to sums of humps and half-cusps thereby measures the mixing parameters of equations (14) and (20). These mixing parameters are the only linear combinations of Lagrangian parameters which can be measured using these cascade decays alone. For stop squark decays, the mixing parameters and any production asymmetry can be separately measured by considering the separate distributions  $b$ - $l^+$  and  $b$ - $l^-$ . For sbottom squark decays, the mixing parameters and the production asymmetry can be separately measured if the  $b$ -quark is signed and the distributions for all four possible combinations of lepton and  $b$  signs are independently examined.

	Hump Process	Weight	Half-Cusp Process	Weight
Opposite-Sign	$\tilde{b}_1^\pm \rightarrow b^\pm \chi_i^0$		$\tilde{b}_1^\pm \rightarrow b^\pm \chi_i^0$	
	$\hookrightarrow b^\pm l^\mp \tilde{l}_L^\pm$	$\sin^2 \alpha_{1i}$	$\hookrightarrow b^\pm l^\mp \tilde{l}_L^\pm$	$\cos^2 \alpha_{1i}$
	$\hookrightarrow b^\pm l^\mp \tilde{l}_R^\pm$	$\cos^2 \alpha_{1i}$	$\hookrightarrow b^\pm l^\mp \tilde{l}_R^\pm$	$\sin^2 \alpha_{1i}$
	$\tilde{b}_2^\pm \rightarrow b^\pm \chi_i^0$		$\tilde{b}_2^\pm \rightarrow b^\pm \chi_i^0$	
	$\hookrightarrow b^\pm l^\mp \tilde{l}_L^\pm$	$\cos^2 \alpha_{2i}$	$\hookrightarrow b^\pm l^\mp \tilde{l}_L^\pm$	$\sin^2 \alpha_{2i}$
	$\hookrightarrow b^\pm l^\mp \tilde{l}_R^\pm$	$\sin^2 \alpha_{2i}$	$\hookrightarrow b^\pm l^\mp \tilde{l}_R^\pm$	$\cos^2 \alpha_{2i}$
	$\tilde{t}_{1,2}^\pm \rightarrow b^\mp \chi_i^\pm$		$\tilde{t}_{1,2}^\pm \rightarrow b^\mp \chi_i^\pm$	
	$\hookrightarrow b^\mp l^\pm \tilde{\nu}_L$	$\cos^2 \beta_{(1,2)i}$	$\hookrightarrow b^\mp l^\pm \tilde{\nu}_L$	$\sin^2 \beta_{(1,2)i}$
Same-Sign	$\tilde{b}_1^\pm \rightarrow b^\pm \chi_i^0$		$\tilde{b}_1^\pm \rightarrow b^\pm \chi_i^0$	
	$\hookrightarrow b^\pm l^\pm \tilde{l}_L^\mp$	$\cos^2 \alpha_{1i}$	$\hookrightarrow b^\pm l^\pm \tilde{l}_L^\mp$	$\sin^2 \alpha_{1i}$
	$\hookrightarrow b^\pm l^\pm \tilde{l}_R^\mp$	$\sin^2 \alpha_{1i}$	$\hookrightarrow b^\pm l^\pm \tilde{l}_R^\mp$	$\cos^2 \alpha_{1i}$
	$\tilde{b}_2^\pm \rightarrow b^\pm \chi_i^0$		$\tilde{b}_2^\pm \rightarrow b^\pm \chi_i^0$	
	$\hookrightarrow b^\pm l^\pm \tilde{l}_L^\mp$	$\sin^2 \alpha_{2i}$	$\hookrightarrow b^\pm l^\pm \tilde{l}_L^\mp$	$\cos^2 \alpha_{2i}$
	$\hookrightarrow b^\pm l^\pm \tilde{l}_R^\mp$	$\cos^2 \alpha_{2i}$	$\hookrightarrow b^\pm l^\pm \tilde{l}_R^\mp$	$\sin^2 \alpha_{2i}$

Table 2: Distributions for the  $b$ - $l$  invariant mass including both gaugino-higgsino mixing and third-generation squark mixing. Here by a slight abuse of notation  $\pm$  distinguishes between (s)quark and anti-(s)quark, so that  $b^\pm$  has charge  $\pm 1/3$ . The relative weights are normalized such that the coefficients for the hump and cusp distributions in a given channel sum to unity. The angles  $\alpha_{ki}, \beta_{ki}$  are defined in equations (14) and (20). The endpoints of the distributions will depend on the masses of the superpartners participating in the cascade.

## 2.2 $b$ -jet signing and measurement of mixings

In practice signing the  $b$ -quark cannot be done with arbitrary purity, and there will be a non-trivial but well-characterized mis-sign rate. In particular there is an irreducible contribution to the mis-sign rate coming from oscillations of the parent  $b$ -quark inside neutral  $B$ -mesons, which is of order 12% [26]. Recent simulations indicate that a mis-sign rate of 15.4% can be achieved, with an efficiency of 1.2% [27]. To measure spin and mixings,  $b$ - $\ell$  distributions should be fit to sums of humps and half-cusps. Let the mis-sign fraction be  $F$ , and consider decay of  $b$ -squarks through neutralinos. If the theoretical distribution in a given channel is

$$D_{theory}(x) = fH(x) + (1 - f)C(x),$$

where  $f$  and  $(1 - f)$  are the (sines and cosines of) angles listed in Table 2, then the experimentally observed distribution is

$$\begin{aligned} D_{obs}(x) &= (1 - F)(fH(x) + (1 - f)C(x)) + F((1 - f)H(x) + fC(x)) \\ &= \hat{f}H(x) + (1 - \hat{f})C(x), \end{aligned} \quad (21)$$

where

$$\hat{f} \equiv f + F - 2fF. \quad (22)$$

Fits to data then directly measure  $\hat{f}$ , which through (22) measures the mixing parameters of equation (14). In a realistic situation there will be a trade-off between purity, that is, minimizing  $F$ , and acceptance. In a full analysis any  $p_T$ -dependence of  $F$  can be included.

In Figure 1 we plot the observable  $b$ - $\ell$  distributions for an intermediate pure bino and  $\cos\theta_b = 0.775$ , assuming no production asymmetry. Two sets of curves are shown. The outer (red) pair are the opposite- and same-sign distributions which would be observed with a 15% mis-sign rate. The inner (blue) pair are the opposite- and same-sign distributions which would be observed with a 30% mis-sign rate. Even with a 30% mis-sign rate the deviation of the distributions from each other and from the triangular distribution is clear, indicating the presence of an intermediate Majorana fermion. Decreasing the mis-sign rate further to 15% significantly enhances the difference between the two channels, and hence the sensitivity to mixing.

Let us finally mention that in the semi-muonic decay modes of the  $b$ , the missing energy carried away by the neutrino alters the energy distribution of the observed  $b$ -jets, and a full analysis must account for this effect. As the polarization of the  $b$ -quark is almost entirely randomized in hadronization [28], the visible spectrum of  $b$ -quark decay products is not dependent on the details of the vertex where the  $b$  originated. The net effect of the loss of the neutrino four-momentum can be described by a convolution of the invariant mass

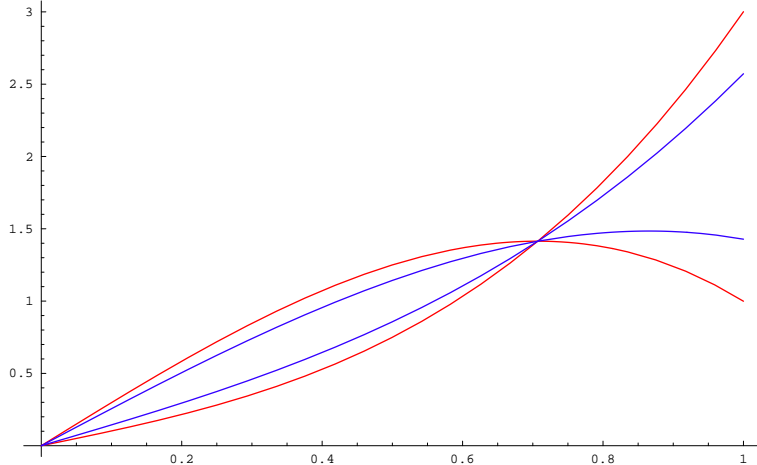


Figure 1: Observable  $b$ - $\ell$  invariant mass distributions arising from  $\tilde{b}$  decay through a neutralino, for  $\cos\theta_b = 0.775$  and intermediate pure bino. The outer (red) pair of curves show the observable distributions assuming a 15% mis-sign rate. The inner (blue) pair of curves show the same distributions assuming a 30% mis-sign rate.

distributions involving the parent  $b$ -quark with a calculable universal transfer function which accounts for the distribution of visible energy in the  $b$ -jets after the loss of the neutrino.

### 3 Ditau and lepton-tau distributions: no mixings

As taus decay within the detector via  $\tau \rightarrow \nu X$ , the full four-momentum of the  $\tau$  is not observable, and events involving final state  $\tau$ s require careful attention to characterize and understand. However, the hadronic decay modes of the  $\tau$  do allow right- and left-handed  $\tau$ s to be distinguished statistically. A left-handed  $\tau$  preferentially emits the neutrino parallel to its direction of motion, resulting in a softer spectrum of visible decay products, while a right-handed  $\tau$  preferentially emits the neutrino anti-parallel to its direction of motion, resulting in a harder spectrum of visible decay products. This difference in the energy distributions of the  $\tau$  daughter products therefore can be used as a handle on the possible chiral couplings of new physics to  $\tau$  leptons [10, 11, 12].

When the  $\tau$  is highly boosted in the lab frame, as it is in most cascade decays, its visible decay products  $d$  are collinear, and to good approximation we can take

$$p_d = zp_\tau,$$

where  $z$  is the fraction of the lab frame  $\tau$  energy carried by the daughters  $d$ ,

$$z = \frac{E_d}{E_\tau}. \quad (23)$$

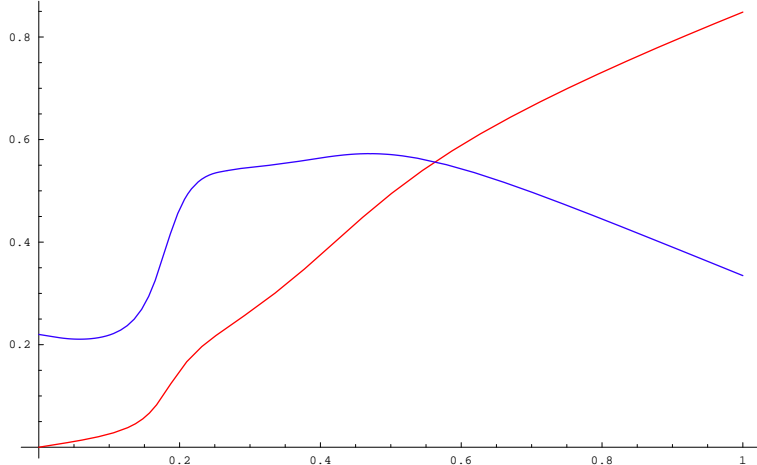


Figure 2: The  $\tau$  daughter energy fraction distributions  $P_{(1)}^{\pm}(z)$  for hadronic one-prong taus, for positive (red) and negative (blue) helicity taus.

The quantity  $z$  is invariant under boosts along the direction of the tau. Also, when the tau is highly boosted, helicity and chirality may be used interchangeably. The distribution of  $z$  is correlated with handedness of the  $\tau$ , as noted above.

At the level of the parent  $\tau$ s, two-step on-shell SUSY cascades can lead to triangle, hump, and half-cusp invariant mass distributions. Intermediate staus, as in the decay chains

$$\chi_i^0 \rightarrow \tau_{L,R}^{\pm} \tilde{\tau}_{L,R}^{\mp} \rightarrow \tau_{L,R}^{\pm} \tau_{L,R}^{\mp} \chi_j^0 \quad (24)$$

give triangles, while the decay chains

$$\tilde{l}_{L,R} \rightarrow \ell \chi_i^0 \rightarrow \ell \tau \tilde{\tau}_{L,R}, \ell \tau \tilde{\tau}_{R,L} \quad (25)$$

and

$$\tilde{\tau}_{L,R} \rightarrow \tau \chi_i^0 \rightarrow \tau \tau \tilde{\tau}_{R,L} \quad (26)$$

yield humps and half-cusps. For final state  $\tau$ 's, these distributions are not directly observable. Rather, we must convolve these distributions with the probability  $P_{(d)}^{\pm}(z)$  that a parent  $\tau$  decays to visible daughter particle(s)  $d$  with momentum fraction  $z = p_d/p_{\tau}$ . The probability  $P_{(d)}^{\pm}$  depends on the helicity of the parent  $\tau$ , denoted  $\pm$ . CP invariance ensures that the energy distributions of a  $\tau$  with a given helicity and its anti-particle are identical. Thus the negative-helicity  $\tau^{-}$  and the positive-helicity  $\tau^{+}$  have identical energy distributions, which we denote by  $P_{(d)}^{-}(z)$  throughout. Similarly, the energy distributions for the positive-helicity  $\tau^{-}$  and its antiparticle, the negative-helicity  $\tau^{+}$ , are given by  $P_{(d)}^{+}(z)$ .

Our analysis uses hadronic one-prong taus as they yield the greatest sensitivity to the tau polarization; our treatment of the one-prong decay mode closely follows that of [12].

We model the energy fraction distributions  $P_{(1)}^\pm(z)$  for one-prong taus by summing the three dominant contributions to this mode, the decays  $\tau^- \rightarrow \nu\pi^0$ ,  $\tau^- \rightarrow \nu\rho^- \rightarrow \nu\pi^-\pi^0$ , and  $\tau^- \rightarrow \nu a_1^- \rightarrow \nu\pi^-\pi^0\pi^0$ . Details of this computation are presented in the Appendix. The total daughter energy fraction distributions  $P_{(1)}^\pm(z)$  that result are shown in Figure 2.

The functions  $P_{(3)}^\pm(z)$  for three-prong taus are comparatively insensitive to tau polarization. The three-prong decay mode is principally due to the decay  $\tau \rightarrow a_1\nu$ , and the total visible energy fraction for the three-prong decay mode is approximately equal to the visible energy fraction contributed by the  $a_1$ 's to the one-prong decay mode. The mass difference between the  $a_1$  and the  $\tau$  is not large, and the contributions of longitudinally and transversely polarized  $a_1$  mesons add to a nearly spin-independent quantity (further details can be found in the Appendix). Therefore including the three-prong decay mode does not increase sensitivity to  $\tau$  polarization in invariant mass distributions<sup>3</sup>.

In lepton-tau final states, the observable invariant mass variable is  $m_{\ell d}$ , where  $d$  again denotes the visible  $\tau$  decay product(s). The variable  $m_{\ell d}^2$  is distributed according to

$$\frac{1}{\Gamma} \frac{d\Gamma}{dm_{\ell d}^2} = \frac{1}{\Gamma} \int_{m_{\ell d}^2}^1 \frac{dz}{z} P_{(d)}^\pm(z) \left. \frac{d\Gamma}{dm_{\ell\tau}^2} \right|_{m_{\ell\tau}^2 = m_{\ell d}^2/z}. \quad (27)$$

In ditau final states, we have similarly

$$\frac{1}{\Gamma} \frac{d\Gamma}{dm_{dd'}^2} = \frac{1}{\Gamma} \int_{m_{dd'}^2}^1 \int_{m_{dd'}^2/z_1}^1 \frac{dz_1}{z_1} P_{(d)}^\pm(z_1) \frac{dz_2}{z_2} P_{(d')}^\pm(z_2) \left. \frac{d\Gamma}{dm_{\tau\tau}^2} \right|_{m_{\tau\tau}^2 = m_{dd'}^2/(z_1 z_2)}. \quad (28)$$

Equations (27) and (28) lead to calculable predictions for the invariant mass distributions of detected tau decay products which will in general depend on the underlying SUSY process, the polarization of the parent tau, and the decay mode(s) selected. We plot invariant mass distributions of this form normalized to unity, rather than to the 45% branching ratio (or the branching ratio squared) into the hadronic one-prong decay modes we model.

Our interest in the rest of this paper will be to explore how information about  $\tau$  polarization can be used in conjunction with invariant mass distributions to further measure properties of a general SUSY model. Our principal aim here is to establish the range of theoretical possibilities.

For the purposes of the remainder of this section, we assume purely chiral couplings, that is, we work in the limit of vanishing left-right stau mixing and Yukawa couplings, and assume that the neutralinos participating in the cascade decays couple purely as gauginos.

---

<sup>3</sup>The three-prong decay modes can, however, be used as an effective polarimeter by examining the distribution of energy among the daughter pions, which is sensitive to the polarization of the  $a_1$ , and therefore to the helicity of the  $\tau$  [14]. Cuts on the relative energy distributions of the daughter hadrons as a way to distinguish between tau polarizations in SUSY cascades have been discussed in [20].

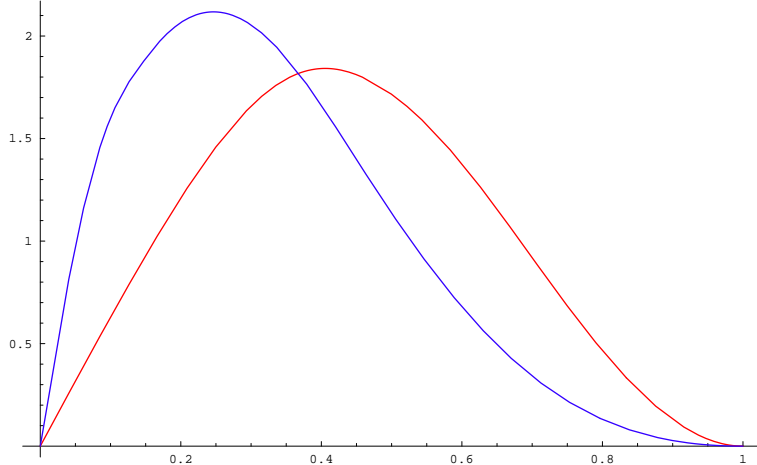


Figure 3: Ditau triangles, for intermediate  $\tilde{\tau}_R$  (red) and intermediate  $\tilde{\tau}_L$  (blue), using one-prong hadronic  $\tau$ s. The distributions are normalized to unity. No mixing.

This is an idealization, and in many well-motivated scenarios left-right stau mixing is appreciable. First we will consider ditau final states, then in section 3.2 move onto lepton-tau final states. Then in section 4 we will incorporate the effects of mixing on both types of final states.

### 3.1 Ditau distributions

Neutralino decay through staus,

$$\chi_i^0 \rightarrow \tau_{L,R}^\pm \tilde{\tau}_{L,R}^\mp \rightarrow \tau_{L,R}^\pm \tau_{L,R}^\mp \chi_j^0, \quad (29)$$

yields a triangular distribution for the ditau invariant mass in the opposite-sign channel. We plot the resulting observable invariant mass distributions of the tau decay products in figure 3. These curves are a result of convolving the underlying triangle distribution with (1)  $P^-(z_1)P^-(z_2)$ , for an intermediate  $\tilde{\tau}_L$ , and (2)  $P^+(z_1)P^+(z_2)$ , for an intermediate  $\tilde{\tau}_R$ . These curves are fairly well separated and it should be possible to clearly distinguish between these two scenarios.

Neutralinos intermediate between two staus lead to an underlying hump distribution in the same-sign channel, simultaneous with an underlying half-cusp distribution in the opposite-sign channel. These humps and half-cusps involve one  $\tau_L$  and one  $\tau_R$  and therefore the observable distributions are obtained by convolution with the  $(+-)$  combination of tau energy transfer functions. The resulting distributions are plotted in figure 4. These distributions must have equal normalization and endpoints. While in practice the upper endpoint may be difficult to discern, this nonetheless translates into a stringent correlation on the relative locations of the peaks in the opposite-sign and same-sign distributions.

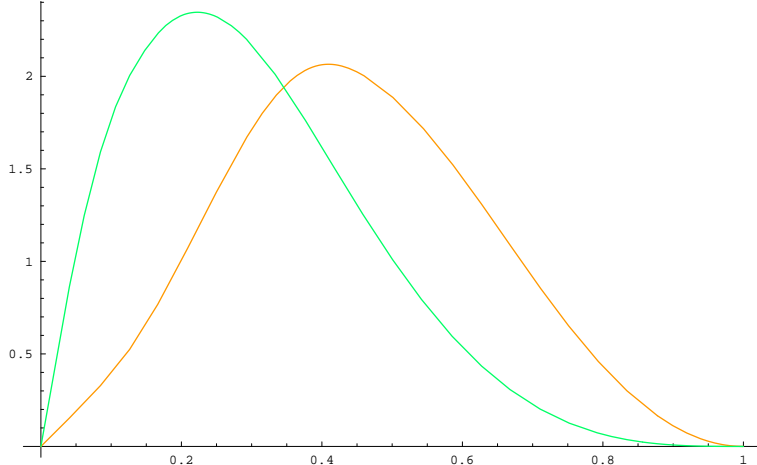


Figure 4: The ditau hump (green) and half-cusp (orange), convolved with the  $(+-)$  combination of energy distribution functions. Using one-prong hadronic  $\tau$ s. No mixing.

An important question is at what level the possible opposite-sign distributions can be distinguished from each other. Toward this end we plot both possible triangle distributions and the half-cusp in Figure 5. While with enough statistics the three curves might possibly be distinguished, on a practical level generating and testing hypotheses to explain an opposite-sign ditau signal will proceed first by cross-channel comparisons. First, if the opposite-sign ditau distribution is an underlying half-cusp, then there should be a corresponding underlying hump distribution in the same-sign channel. The absence of a same-sign signal strongly suggests that the opposite-sign signal is an underlying triangle distribution, due to intermediate staus. In addition, opposite-sign triangles and opposite-sign half-cusps fit into hypotheses which make different predictions for object counts in the rest of the signal events. In particular, if the opposite-sign signal is due to half-cusps, then there should be a larger number of leptons in the event (most likely  $\tau$ 's) coming from decays into the  $\tilde{\tau}$  initiating the decay chain, and from subsequent decay of the  $\tilde{\tau}$  terminating the decay chain. These additional  $\tau$ 's will naturally present some combinatorial complications, which again we will not address here.

### 3.2 Lepton-tau distributions

Lepton-tau distributions arise from slepton decay to a stau through a neutralino,

$$\tilde{l}_{L,R} \rightarrow \ell \chi_i^0 \rightarrow \ell \tau \tilde{\tau}_{L,R}, \ell \tau \tilde{\tau}_{R,L},$$

or the analogous process with initial stau and final slepton. In the absence of mixing, there are four possible observable distributions in lepton-tau channels, namely the hump convolved with the  $(+)$  energy distribution function; the hump convolved with the  $(-)$  energy

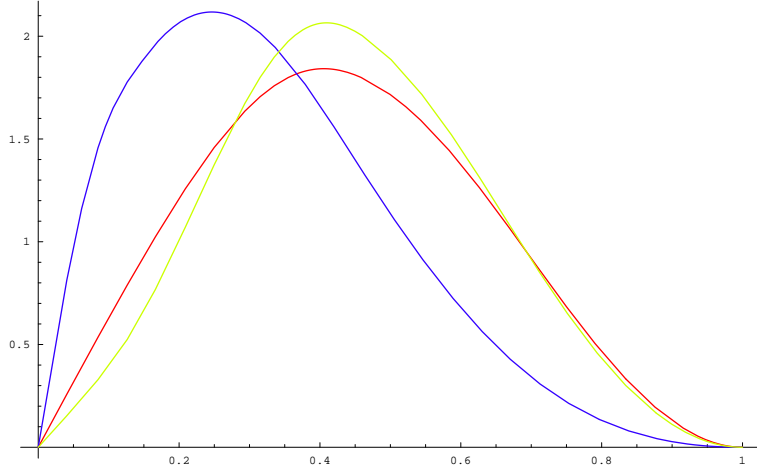


Figure 5: Opposite sign ditau distributions: both possible triangle distributions (with tau polarizations  $(++)$  in red and  $(--)$  in blue), plotted against the half-cusp (with tau polarizations  $(+-)$ , in orange). Using one-prong hadronic  $\tau$ s. No mixing.

distribution function; the half-cusp convolved with the  $(+)$  energy distribution function; and the half-cusp convolved with the  $(-)$  energy distribution function. These distributions are plotted in Figure 6. Depending on the handedness of both the slepton and the stau participating in the decay chain, all of these shapes may appear in either the same-sign channel or the opposite-sign channel, as we summarize in Table 3. Note that, for any given process, there is a specific prediction for which of the four shapes must appear in the same-sign channel and which must appear in the opposite-sign channel. They must have the same normalization, and the same endpoints. In addition it is worth pointing out that the helicity of the tau in both the opposite-sign and same-sign channels is the same.

It should be readily possible to distinguish whether the cusp distribution occurs in the same-sign or the opposite-sign channel, as even after convolution the hump and half-cusp distributions are fairly distinct. *This allows one to distinguish between the scenario where the slepton and the stau have the same handedness, and the scenario where the slepton and the stau have opposite handedness.* To proceed further one would like to identify the handedness of the stau and therefore of the slepton. This requires comparing the  $C_R$  distribution to the  $C_L$  distribution, and likewise between the  $H_R$  and the  $H_L$  distributions. While this may be challenging for the humps, the cusps are more distinct. The discriminatory power is enhanced by the existence of two channels which must both have the same polarization. With enough statistics we expect that the identity of the stau and therefore of the slepton can be discerned.

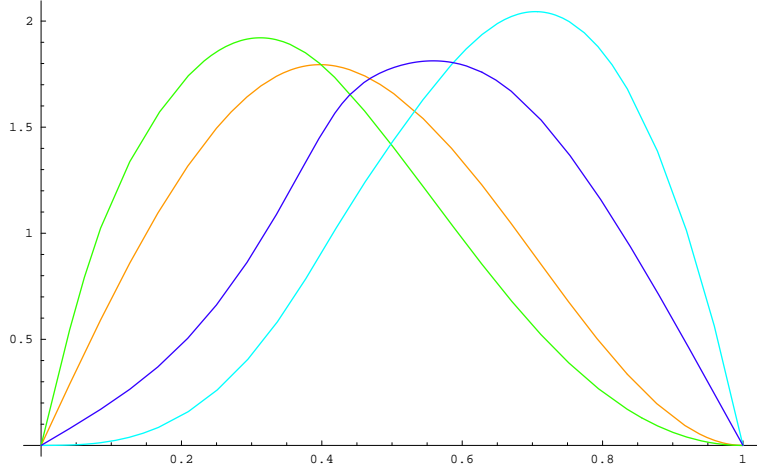


Figure 6: All four possible lepton-tau distributions: the hump with negative (green) and positive (orange) polarizations, the cusp with negative (blue) and positive (cyan) polarizations. Using one-prong hadronic  $\tau$ s. No mixing.

Process	Same-Sign	Opposite-Sign
$\tilde{l}_R \rightarrow \ell\tau\tilde{\tau}_R$	$C_R$	$H_R$
$\tilde{l}_R \rightarrow \ell\tau\tilde{\tau}_L$	$H_L$	$C_L$
$\tilde{l}_L \rightarrow \ell\tau\tilde{\tau}_R$	$H_R$	$C_R$
$\tilde{l}_L \rightarrow \ell\tau\tilde{\tau}_L$	$C_L$	$H_L$

Table 3: Possible lepton-tau distributions in the absence of mixing. Here we denote by  $C_R$  the half-cusp distribution convolved with the positive polarization energy distribution function, and by  $H_L$  the hump distribution convolved with the negative polarization energy distribution function. Identical conclusions pertain if the roles of the stau and the slepton are reversed. An experimental determination of the channel in which the half-cusp and hump distributions appear determines the relative handedness of the slepton and stau.

## 4 Ditau and lepton-tau distributions in the presence of mixing

In many realistic SUSY models, mixing in the tau sector is nonnegligible. As left- and right-handed  $\tau$ 's have different daughter energy spectra, the observable invariant mass distributions will be a weighted sum of the distributions for purely left- and purely right-handed  $\tau$ s, with weights determined by the mixing parameters. In addition, as we saw with  $b$ - $l$  distributions in section 2, reducing the chirality of the fermion-sfermion-neutralino vertices serves to wash out angular correlations from intermediate fermions. A careful fit of observed tau distributions therefore has the potential to probe the chiral structure and mixings of the new physics.

The Yukawa interactions between the two stau mass eigenstates, the  $i^{\text{th}}$  neutralino, and the right and left-handed taus are

$$\mathcal{L}_{int} = \tilde{\tau}_1 \left( \tau_R \chi_i^0 y_{1,i}^R + (\chi_i^0)^\dagger \tau_L^\dagger y_{1,i}^L \right) + \tilde{\tau}_2 \left( \tau_R \chi_i^0 y_{2,i}^R + (\chi_i^0)^\dagger \tau_L^\dagger y_{2,i}^L \right) + \text{H.c.} \quad (30)$$

(In our conventions,  $\tau_R$  is a left-handed anti-tau.) The stau-tau-neutralino Yukawa couplings are

$$y_{1,i}^R = \sin \theta_{\tilde{\tau}} \lambda_\tau U_{di}^* + \cos \theta_{\tilde{\tau}} \sqrt{2} g' U_{Bi}^* \quad (31)$$

$$y_{1,i}^L = \sin \theta_{\tilde{\tau}} \left( -\frac{g}{\sqrt{2}} U_{iW} - \frac{g'}{\sqrt{2}} U_{iB} \right) + \cos \theta_{\tilde{\tau}} \lambda_\tau U_{di} \quad (32)$$

$$y_{2,i}^R = \cos \theta_{\tilde{\tau}} \lambda_\tau U_{di}^* - \sin \theta_{\tilde{\tau}} \sqrt{2} g' U_{Bi}^* \quad (33)$$

$$y_{2,i}^L = \cos \theta_{\tilde{\tau}} \left( -\frac{g}{\sqrt{2}} U_{iW} - \frac{g'}{\sqrt{2}} U_{iB} \right) - \sin \theta_{\tilde{\tau}} \lambda_\tau U_{di} \quad (34)$$

with the property that  $y_{2,i}^L \rightarrow 1, y_{1,i}^R \rightarrow 1, y_{1,i}^L \rightarrow 0, y_{2,i}^R \rightarrow 0$  as the both the stau and neutralino mixings are turned off, that is, as  $\theta_{\tilde{\tau}}, U_{di} \rightarrow 0$ . The combinations of these parameters which enter into the observable distributions are the relative probabilities of producing right- and left-handed taus at each vertex,

$$\cos^2 \phi_{1,i} \equiv \frac{|y_{1,i}^R|^2}{|y_{1,i}^R|^2 + |y_{1,i}^L|^2} \quad (35)$$

$$\cos^2 \phi_{2,i} \equiv \frac{|y_{2,i}^L|^2}{|y_{2,i}^L|^2 + |y_{2,i}^R|^2} \quad (36)$$

### 4.1 Ditau triangles

Consider first the FSF process, neutralino to stau to neutralino. This gives a ditau ‘‘triangle’’. It is possible now for each  $\tau$  to be either positively or negatively polarized, with a probability depending on the mixings in both the neutralino and the stau sectors.

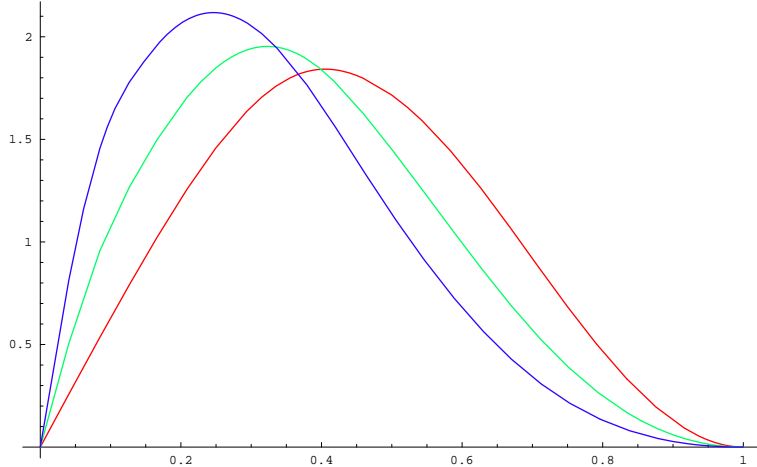


Figure 7: All three possible ditau triangles:  $T_{LL}$  (blue),  $T_{LR} = T_{RL}$  (green), and  $T_{RR}$  (red). Using one-prong hadronic  $\tau$ s. All curves have the same normalization and endpoints.

The general distribution for this process is a sum of three possible fundamental shapes, corresponding to the triangle distribution convolved with the three different combinations of tau polarizations,  $T_{LL}, T_{LR}, T_{RR}$ . These shapes are plotted in Figure 7. For general mixings, the cascade  $\chi_j^0 \rightarrow \tilde{\tau}_1 \tau \rightarrow \tau \tau \chi_i^0$  now gives the invariant mass distribution

$$\begin{aligned}
 D(x) = & \cos^2 \phi_{1,i} \cos^2 \phi_{1,j} T_{RR}(x) \\
 & + (\cos^2 \phi_{1,i} \sin^2 \phi_{1,j} + \sin^2 \phi_{1,i} \cos^2 \phi_{1,j}) T_{LR}(x) \\
 & + \sin^2 \phi_{1,i} \sin^2 \phi_{1,j} T_{LL}(x).
 \end{aligned}
 \tag{37}$$

This defines a two-parameter family of distributions. In principle one could fit the observed ditau invariant mass distribution to this formula, using a two-parameter fit. This would measure the mixings in the stau and neutralino sectors as well as the helicities of the taus. Such an analysis is difficult, however, as the fit is not completely straightforward. First, the distribution  $T_{LR}$  only differs from the average  $(T_{LL} + T_{RR})/2$  by a few percent. Second, it is difficult in practice to accurately locate the upper endpoint of these distributions. We now discuss a method of analysis which deals with these two issues.

The ditau distributions are weighted towards smaller invariant mass,  $x \lesssim 0.5$ , even for underlying half-cusp or triangle distributions which peak at large invariant mass, due to the energy lost to neutrinos. An unfortunate consequence of this feature is that the upper endpoints are poorly defined for many of these distributions, as can be seen in Figures 7, 9, and 10. Anchoring the distributions by their endpoints may then not be feasible experimentally. The most visible feature of all of these distributions is not the upper endpoint but rather the location of the maximum. Moreover, the shape and relative location of the maxima are distinct features of the various distributions. A reliable way to

fit experimental data to (sums of) these distributions is thus to fit to the location of the peak, rescaling the normalizations to preserve the total area of the distributions—that is, the total number of events—while allowing the relative locations of the endpoints to vary. Given a measured ditau distribution with a peak located at invariant mass

$$m_{hh'} = m_{peak}, \quad (38)$$

the experimental data can be compared to theoretical distributions rescaled to have the same peak location.

To do this, consider a generic ditau distribution  $T_{\{a\}}(x)$  which is a linear combination of the basic theoretical distributions  $T_{LL}$ ,  $T_{RR}$  and  $T_{LR}$ ,

$$T_{\{a\}}(x) = a_{LL}T_{LL}(x) + a_{RR}T_{RR}(x) + a_{LR}T_{LR}(x).$$

This distribution  $T_{\{a\}}(x)$  has a maximum at a fixed numerical value  $x_{peak} \equiv c_{\{a\}}$ , which is uniquely determined by the coefficients  $a_{LL}$ ,  $a_{RR}$  and  $a_{LR}$ . Recall that the scaled variable  $x$  is the ratio of the invariant mass to the endpoint,

$$x = \frac{m_{hh'}}{m_{end}}.$$

If the (scaled) theoretical distribution  $T_{\{a\}}(x)$  is to describe the data with a peak at  $m_{peak}$ , it must have an endpoint at  $m_{end} = m_{peak}/c_{\{a\}}$ . Define a new variable  $y$  which is scaled by the visible location of the peak, rather than the location of the endpoint:

$$y \equiv \frac{x}{c_{\{a\}}} = \frac{m_{hh'}}{c_{\{a\}}m_{end}} = \frac{m_{hh'}}{m_{peak}}.$$

In terms of  $y$ , the properly normalized theoretical distributions to fit to data are

$$P_{\{a\}}(y) = c_{\{a\}}T_{\{a\}}(c_{\{a\}}y), \quad (39)$$

where  $\int_0^{1/c_{\{a\}}} dy P_{\{a\}}(y) = 1$ . By construction all distributions  $P_{\{a\}}$  have a peak at the same location. The three rescaled triangle distributions are plotted in Figure 8.

This rescaling procedure maximizes the distinguishability of the different possible distributions and allows the fit to be performed without any knowledge about the location of the endpoint in the experimentally observed distributions. However, it does require backgrounds to be well-characterized, as the total number of events needs to be well understood.

We now address the approximate degeneracy between  $T_{LR}$  and  $(T_{LL} + T_{RR})/2$ . Writing  $\sin^2 \phi_{1,j} = w_j$ , equation (37) can be rewritten

$$D(x) = T_{RR}(x) + (w_1 + w_2)(T_{LR} - T_{RR}) + w_1w_2(T_{RR} + T_{LL} - 2T_{LR}). \quad (40)$$

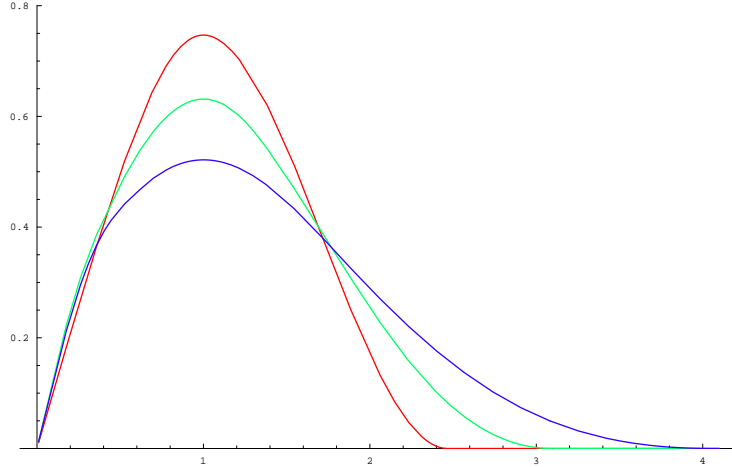


Figure 8: The three possible ditau triangles:  $T_{LL}$  (blue),  $T_{LR} = T_{RL}$  (green), and  $T_{RR}$  (red), rescaled to have the same normalization and location of peak. Using one-prong hadronic  $\tau$ s.

The final term in parentheses can be neglected, subject to the limits of experimental precision. Moreover, this term is multiplied by a coefficient quadratic in  $w_j$ . If the angles  $\phi_{1,j}$  are small—so that the  $\tau$ 's being produced are predominantly right-handed—then the final term in equation (40) is doubly small. The experimental data can then be fit to

$$\hat{D}(x) = T_{RR}(x) + (w_1 + w_2)(T_{LR} - T_{RR}) \quad (41)$$

using a one-parameter fit. This is a useful parameterisation when one suspects that the taus being produced are mostly positively polarized, as one would be able to learn from an examination of the relative energy carried by charged and neutral hadrons in the reconstructed taus. If the taus are mostly left-handed then a more useful parameterization of equation (37) is obtained by taking  $\cos^2 \phi_{1,j} = w_j$ , and fitting to the resulting approximate distribution

$$\check{D}(x) = T_{LL}(x) + (w_1 + w_2)(T_{LR} - T_{LL}). \quad (42)$$

Of course, in an intermediate situation the parameterization  $\cos^2 \phi_{1,1} = w_1, \cos^2 \phi_{1,2} = 1 - w_2$  may be more convenient. In all of these cases the fit measures the sum of the relative probabilities of producing right-handed versus left-handed taus at both vertices.

## 4.2 Ditau humps and half-cusps in the presence of mixing

In the presence of mixing, the cascade

$$\tilde{\tau}_2 \rightarrow \tau \chi_i^0 \rightarrow \tau \tau \tilde{\tau}_1 \quad (43)$$

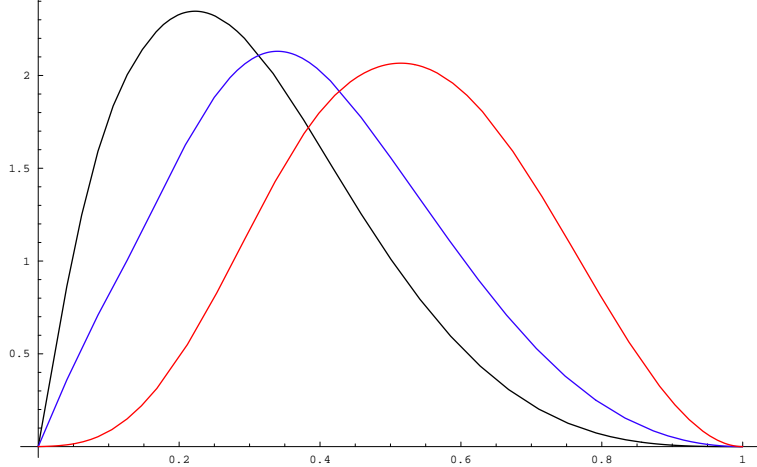


Figure 9: The three distributions which contribute to the same-sign ditau distribution:  $H_{LR}$  (black),  $C_{LL}$  (blue), and  $C_{RR}$  (red). Using one-prong hadronic  $\tau$ s. All curves have the same normalization and endpoints.

now gives the invariant mass distribution

$$D_{SS}(x) = (\cos^2 \phi_{1,i} \cos^2 \phi_{2,i} + \sin^2 \phi_{1,i} \sin^2 \phi_{2,i})H_{LR}(x) + \cos^2 \phi_{1,i} \sin^2 \phi_{2,i} C_{RR} + \sin^2 \phi_{1,i} \cos^2 \phi_{2,i} C_{LL}(x) \quad (44)$$

in the same-sign channel, and the distribution

$$D_{OS}(x) = (\cos^2 \phi_{1,i} \cos^2 \phi_{2,i} + \sin^2 \phi_{1,i} \sin^2 \phi_{2,i})C_{LR}(x) + \cos^2 \phi_{1,i} \sin^2 \phi_{2,i} H_{RR} + \sin^2 \phi_{1,i} \cos^2 \phi_{2,i} H_{LL}(x) \quad (45)$$

in the opposite-sign channel. As we have discussed above, object counts and cross-channel correlations will likely first be used to distinguish between FSF scenarios and SFS scenarios, so for the moment we concentrate on the mixing-induced modifications to the ditau distributions which result from the process (43) alone. The three distributions which appear in equation (44) are plotted in Figure 9. The distribution  $H_{LR}$ , which would appear in the limit of no mixing, is shown in black, and the mixing-induced contributions  $C_{LL}$  and  $C_{RR}$  are shown in blue and red respectively. Similarly, the three distributions which appear in equation (45) are plotted in Figure 10. The distribution  $C_{LR}$  is shown in black, and the mixing-induced contributions  $H_{LL}$  and  $H_{RR}$  in blue and red respectively.

To compare the distributions to data we rescale the distributions to fit the location of the peak and the total number of events, as with the triangles. The rescaled distributions are plotted in Figures 11 and 12. Unlike the triangles, all three curves in each channel are distinct enough to allow the possibility of a full two-parameter fit, although high statistics would be required. In addition one is able to perform the same measurement in both the

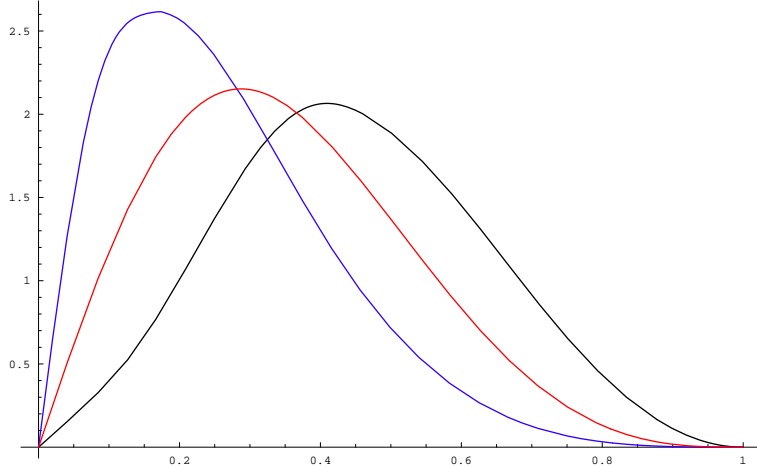


Figure 10: The three distributions which contribute to the opposite-sign ditau distribution:  $C_{LR}$  (black),  $H_{LL}$  (blue), and  $H_{RR}$  (red). Using one-prong hadronic  $\tau$ s. All curves have the same normalization and endpoints.

opposite-sign and same-sign channel. In this case the probabilities of producing right- and left-handed taus at each vertex could separately be measured, in principle. In practice, any measurement of this sort would require a good strategy for dealing with the combinatorial complications of additional  $\tau$ s in the event, as well as the likely presence of opposite-sign ditau triangle distributions in addition to the opposite-sign (mixed) half-cusp of (45).

### 4.3 Lepton-tau distributions with mixing

The possible lepton-tau distributions in the absence of mixing are listed in Table 3. Once mixing is turned on, a channel which began with a hump (half-cusp) distribution and a given polarization in the absence of mixing will also have a contribution of the half-cusp (hump) distribution, convolved with the opposite polarization. Thus, for instance, the process

$$\tilde{l}_R \rightarrow l\tau\tilde{\tau}_1$$

gives the distribution

$$D_{OS} = \cos^2 \phi_{1,i} H_R(x) + \sin^2 \phi_{1,i} C_L(x)$$

in the opposite-sign channel, and the distribution

$$D_{SS} = \cos^2 \phi_{1,i} C_R(x) + \sin^2 \phi_{1,i} H_L(x).$$

As there is only one  $\tau$  vertex, this is only a one-parameter fit. The result of the fit is the relative probability of emitting right- versus left-handed taus at the tau-stau-neutralino

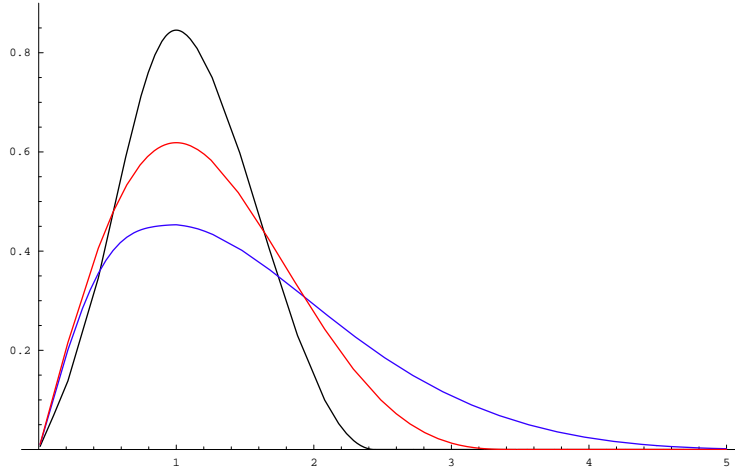


Figure 11: The three distributions which contribute to the opposite-sign ditau distribution:  $C_{LR}$  (black),  $H_{LL}$  (blue), and  $H_{RR}$  (red), rescaled to have the same normalization and location of peak. Using one-prong hadronic  $\tau$ s.

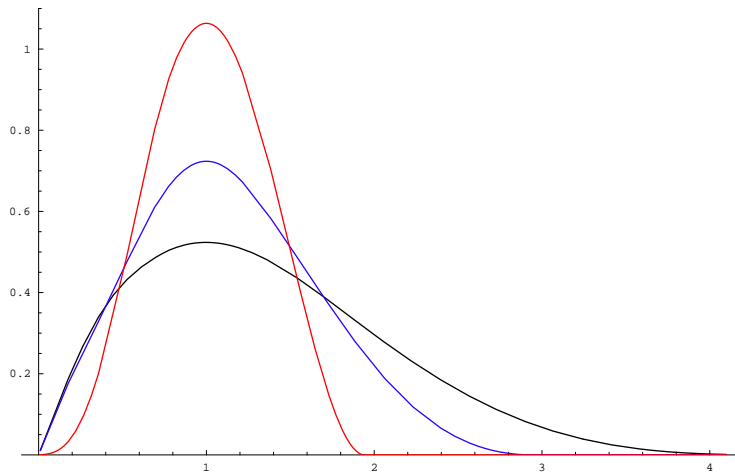


Figure 12: The three distributions which contribute to the same-sign ditau distribution:  $H_{LR}$  (black),  $C_{LL}$  (blue), and  $C_{RR}$  (red), rescaled to have the same normalization and location of peak. Using one-prong hadronic  $\tau$ s.

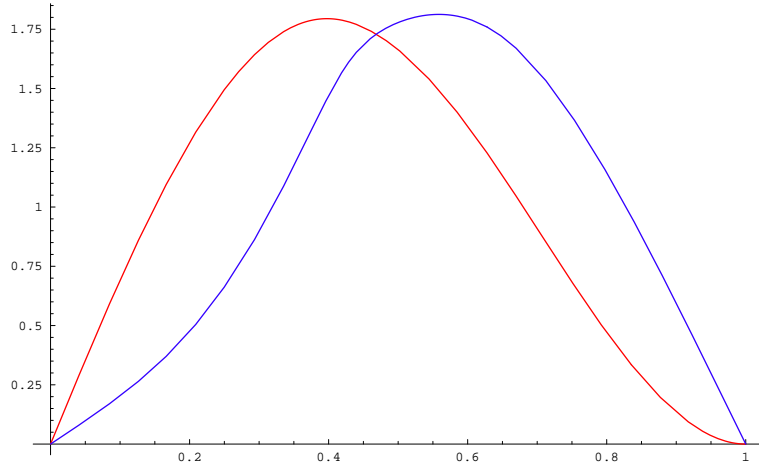


Figure 13: The distributions  $H_R(x)$  (red) and  $C_L(x)$  (blue). Using one-prong hadronic  $\tau$ s.

vertex; the opposite-sign and same-sign channels independently constrain this probability. Notice that the lepton-tau distributions appear in pairs: in any given channel, the distribution must be a weighted sum either of  $H_R(x)$  and  $C_L(x)$  or of  $H_L(x)$  and  $C_R(x)$ . There remains the discrete ambiguity of which of these pairs of distributions occurs in the same-sign and which in the opposite-sign channel. However, as the lepton-tau distributions are more distinct from one another, and as less energy is lost to neutrinos, one scenario should be clearly preferred.

In Figures 13 and 14 we plot the two separate combinations of lepton-tau distributions which can appear in any given channel. Compared to the ditau distributions, the peaks of these distributions are broader, and the endpoints of these distributions are more distinct. In these channels, fits which anchor the endpoint of the distribution rather than the peak may yield better results. For comparison we plot the rescaled distributions with identical peak locations in Figures 15 and 16.

## 5 Conclusions

We have categorized the possible  $b$ - $l$ ,  $\tau$ - $l$ , and  $\tau$ - $\tau$  invariant mass distributions which can arise from two-step on-shell SUSY cascade decays and outlined several ways in which the special properties of  $b$ 's and  $\tau$ 's can be used to probe detailed properties of the underlying MSSM Lagrangian.

In the MSSM,  $b$ - $l$  distributions arise from the decay of a squark through a neutralino or chargino to a slepton. The interplay between the nontrivial spin of the intermediate fermion and the chiral vertices leads to a rich structure of invariant mass distributions. The

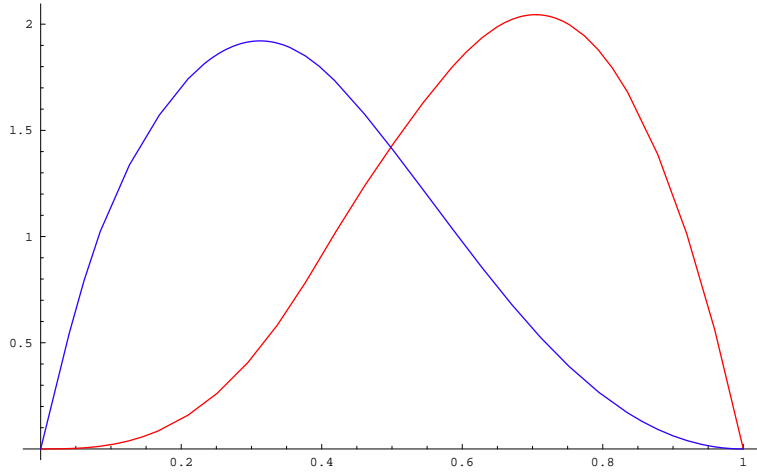


Figure 14: The distributions  $C_R(x)$  (red) and  $H_L(x)$  (blue). Using one-prong hadronic  $\tau$ s.

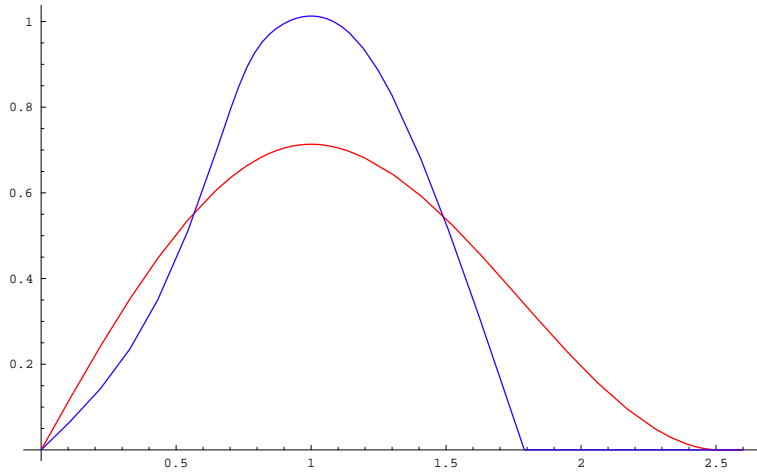


Figure 15: The distributions  $H_R(x)$  (red) and  $C_L(x)$  (blue), rescaled to have the same normalization and location of peak. Using one-prong hadronic  $\tau$ s.

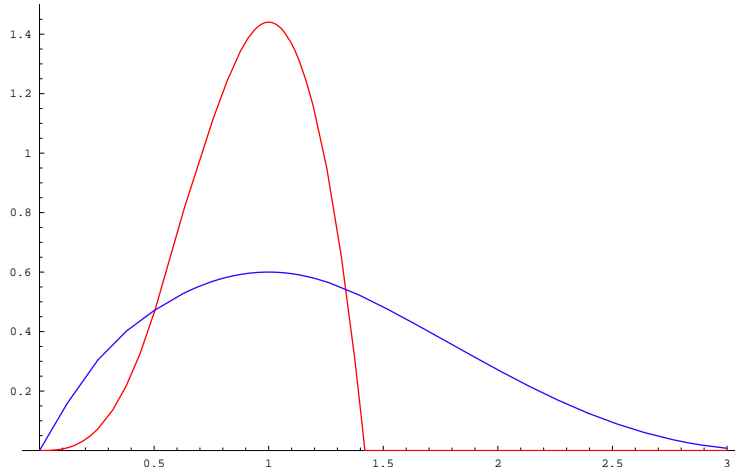


Figure 16: The distributions  $C_R(x)$  (red) and  $H_L(x)$  (blue), rescaled to have the same normalization and location of peak. Using one-prong hadronic  $\tau$ s.

distinctive structure of the invariant mass distribution arising from stop decay through a chargino establishes the spin of the chargino and depends on the mixings in the chargino-stop sector. Signing the  $b$ -jet further allows the separate contributions of the two helicity states of a Majorana neutralino to be resolved, and opens the door to measurements of the neutralino spin and mixings in the sbottom-neutralino sector.

Invariant mass distributions for final state  $\tau$ s depend on the polarization of the  $\tau$ . For analyses using invariant mass distributions only, hadronic one-prong  $\tau$ s provide the greatest sensitivity to  $\tau$  polarization. We have used a semi-analytic model of the one-prong decay mode incorporating  $\tau$  decays to  $\pi$ ,  $\rho$ , and  $a_1$ , which together account for 90% of all one-prong  $\tau$ 's. With this model we computed the possible theoretical distributions for the observable  $\tau$ - $l$  and  $\tau$ - $\tau$  invariant masses.

The ditau triangle distribution has excellent prospects for yielding detailed measurements under realistic conditions, due in part to the minimal combinatorial confusion in such events. Precision fits of the ditau triangle can directly establish the handedness of the intermediate stau and measure mixings in the stau-neutralino sector. This fit is not completely straightforward as, due to the two missing neutrinos, the upper endpoint of the ditau triangle distribution is difficult to discern. The peak of the ditau triangle is more readily located, and we have proposed an algorithm which fits ditau distributions to the location of the peak, rather than the location of the endpoint.

The distributions which we have examined here are uniquely sensitive to spins and mixings and present several interesting possibilities for measurements. Much more work is necessary, however, in order to assess when and how well such measurements can actually be made in realistic circumstances. One of the chief obstacles to fully utilizing the

correlations identified here is the combinatorial confusion associated with identifying the correct pairing of objects in an event. Without a good strategy to minimize this ambiguity, the ability of (e.g.)  $b$ - $l$  invariant mass distributions to determine neutralino spin is greatly reduced. As an acceptance price must be paid for signing the  $b$ -jets, cuts to reduce combinatorial background must be applied with care in order not to run out of signal. However, there are several possible approaches to reducing the combinatorial background and we are optimistic about the possibilities of performing interesting spin and mixing measurements under realistic conditions. We intend to return to this point in future work.

In our systematic consideration of  $b$ - $l$ ,  $\tau$ - $l$ , and  $\tau$ - $\tau$  invariant mass distributions, we have mapped out the space of possibilities for what shapes and intercorrelations of these distributions can appear, and for which combinations of parameters these distributions can probe. We consider it instructive to understand which of these many possibilities have been realized in benchmark models, and hope that the present work can help guide future studies.

## 6 Appendix

$\tau$  decays to a single charged particle (plus any number of neutral particles) constitute 84.7% of all  $\tau$  decays. Included in this 84.7% is the leptonic branching fraction, 35.2% of all  $\tau$  decays, into the final states  $e\bar{\nu}_e\nu_\tau$  and  $\mu\bar{\nu}_\mu\nu_\tau$ . The remaining 49.5% of all  $\tau$  decays are hadronic one-prong  $\tau$ s. Three-prong  $\tau$ 's contribute another 15.2%. All branching fractions are taken from the PDG [26].

Hadronic one-prong  $\tau$ s offer the most sensitive polarimeter for polarization analyses using invariant mass distributions and are the focus of the present work. The dominant contributions to the hadronic one-prong decay mode come from

- $\tau^- \rightarrow \nu\pi^-$ : the branching fraction into this mode is 11.1%.
- $\tau^- \rightarrow \nu\rho^- \rightarrow \nu\pi^-\pi^0$ : the branching fraction into this mode is 25.4%.
- $\tau^- \rightarrow \nu a_1^- \rightarrow \nu\pi^-\pi^0\pi^0$ : the branching fraction into this mode is more difficult to estimate. By isospin, this mode is related to the three-prong decay mode  $\tau^- \rightarrow \nu a_1^- \rightarrow \nu\pi^-\pi^-\pi^+$ . The total branching fraction into this final state, with no additional neutrals, is approximately 9%. We take this to be our estimate of the total branching fraction of  $\tau^- \rightarrow \nu a_1^- \rightarrow \nu\pi^-\pi^0\pi^0$ .

These three decay modes contribute a branching fraction of 45% to all tau decays, leaving a total branching fraction of 5% into one-prong taus from other modes, e.g. modes including

kaons and continuum modes with no identifiable intermediate hadronic resonance. We model the hadronic one-prong  $\tau$ s as the sum of the contributions from the three decay modes listed above. This incorporates 90% of the contributions to the one-prong mode, and provides a good approximation to the full hadronic one-prong  $\tau$ s. Incorporating the intermediate vector mesons  $\rho, a_1$  is important as the thresholds associated with the masses and widths of these particles lead to notable features in the visible hadronic energy spectra of polarized  $\tau$ s.

A full experimental study would be done with TAUOLA [29], which incorporates all measured contributions to the  $\tau$  decay modes.

The matrix elements for the process  $\tau \rightarrow \nu\pi$  depend on the polarization  $\pm$  of the parent  $\tau$ . They are given by (we drop overall constants)

$$\check{\mathcal{M}}_+ = \cos \frac{\theta}{2} \tag{46}$$

$$\check{\mathcal{M}}_- = \sin \frac{\theta}{2}, \tag{47}$$

where  $\theta$  is the angle between the pion and the  $\tau$  axis of polarization in the  $\tau$  rest frame. Squaring the matrix element and integrating over final state phase space, we obtain

$$\frac{1}{\Gamma} \frac{d\Gamma}{d \cos \theta} = \frac{1}{2} (1 + \mathcal{P}_\tau \cos \theta),$$

where  $\mathcal{P}_\tau = \pm$  is the polarization of the  $\tau$ . These angular distributions can be simply understood by appealing to angular momentum conservation: the left-handed neutrino must carry off the total angular momentum of the  $\tau$ , and is therefore emitted forward for initial left-handed  $\tau$ s, and backward for initial right-handed  $\tau$ s.

The  $\tau$ s produced at colliders are typically highly boosted, and the variable of interest is not  $\theta$  but rather  $z$ , the fraction of the  $\tau$  (lab frame) energy which is carried by the hadronic daughters,

$$z \equiv \frac{E_d}{E_\tau}.$$

In the collinear approximation this quantity is invariant under boosts along the  $\tau$ 's direction of motion. In terms of the (unknown) boost  $\beta$  between the  $\tau$  rest frame and the lab frame,

$$\cos \theta = \frac{2z - 1 - (m_\pi^2/m_\tau^2)}{\beta(1 - (m_\pi^2/m_\tau^2))}. \tag{48}$$

We will henceforth work in the collinear limit,  $\beta \rightarrow 1$ . Taking this limit and dropping the factor  $m_\pi^2/m_\tau^2$ , we obtain for the pion spectra

$$P_{(\pi)}^\pm(z) = 1 \pm (2z - 1).$$

The decay modes  $\tau^- \rightarrow \nu\rho^-$ ,  $\tau^- \rightarrow \nu a_1^-$  are more complicated, due to the different contributions from the longitudinal and transverse polarizations of the vector mesons, and the finite widths of the intermediate states.

The matrix elements governing  $\tau$  decay to  $\nu v^\mu$  depend on the polarization  $\pm$  of the parent  $\tau$  as well as the polarization  $T, L$  of the vector meson  $v^\mu$ . These matrix elements are (we again drop overall constants independent of  $m_v$ )

$$\begin{aligned}\check{\mathcal{M}}_{-T} &= \sqrt{2(m_\tau^2 - m_v^2)} \cos \frac{\theta}{2} & \check{\mathcal{M}}_{-L} &= \frac{m_\tau}{m_v} \sqrt{(m_\tau^2 - m_v^2)} \sin \frac{\theta}{2} \\ \check{\mathcal{M}}_{+T} &= -\sqrt{2(m_\tau^2 - m_v^2)} \sin \frac{\theta}{2} & \check{\mathcal{M}}_{+L} &= \frac{m_\tau}{m_v} \sqrt{(m_\tau^2 - m_v^2)} \cos \frac{\theta}{2}\end{aligned}\quad (49)$$

where  $\theta$  is the angle between the vector meson and the  $\tau$  axis of polarization in the  $\tau$  rest frame. Note the longitudinal polarization  $L$ , which carries zero angular momentum along the tau polarization axis in the tau rest frame, contributes like the scalar pion, while the transverse polarization  $T$  contributes oppositely. (Note also that angular momentum conservation allows only one of the two transverse polarizations to contribute to the decay.) In the narrow width approximation, the net distribution of events in  $\cos\theta$  is then of the form [10]

$$\frac{1}{\Gamma} \frac{d\Gamma}{d\cos\theta} = \frac{1}{2} \left( 1 + \mathcal{P}_\tau \left( \frac{m_\tau^2 - 2m_v^2}{m_\tau^2 + 2m_v^2} \right) \cos\theta \right).$$

In other words, the two different vector meson polarizations make contributions to the  $\tau$  helicity-dependent portion of the amplitude which tend to cancel. The factor  $(m_\tau^2 - 2m_v^2)/(m_\tau^2 + 2m_v^2)$  is approximately 0.45 for the  $\rho$ , and only 0.03 for the  $a_1$ . Thus, with no discrimination between the separate contributions of longitudinal and transverse  $a_1$ s, the  $a_1$ s do not yield much sensitivity to  $\tau$  polarization.

In order to obtain a realistic spectrum of hadronic daughter energies, the finite widths of the intermediate vector mesons  $\rho$ ,  $a_1$  must be taken into account. Following [12], we use a Breit-Wigner distribution for the vector mesons, incorporating a running width  $\Gamma_v(m^2)$ , as we now detail.

In general the contribution to the decay distribution from the intermediate vector meson  $v$  takes the form

$$d\Gamma \propto \int d\Pi_2(\tau \rightarrow \nu v) dm_v^2 d\Pi_n(v \rightarrow n\pi) |\check{\mathcal{M}}_\mu(\tau \rightarrow \nu v) \mathcal{P}_v^{\mu\nu}(m_v^2) \hat{\mathcal{M}}_\nu(v \rightarrow n\pi)|^2.$$

Here  $\mathcal{P}_v^{\mu\nu}(m_v^2)$  is the vector meson propagator. It is convenient to write the total matrix element for this process as a sum of contributions from the longitudinal and transverse polarizations of the intermediate vector meson  $v$ . After integrating over the  $n$ -pion phase space, the interference between the vector meson polarizations vanishes and the decay rate

given above greatly simplifies. It is natural to define the lineshape (or vector meson decay rate)

$$g_v(m_v^2) = \int d\Pi_n(v \rightarrow n\pi) |\hat{\mathcal{M}}(v \rightarrow n\pi)|^2,$$

which does not depend on polarization. By the optical theorem the lineshape is proportional to the running width of the vector meson,

$$m_v \Gamma_v(m_v^2) \propto g_v(m_v^2).$$

The decay distribution can now be written

$$d\Gamma \propto \int d\Pi_2(\tau \rightarrow \nu\nu) dm_v^2 \left( |\check{\mathcal{M}}_L(\tau \rightarrow \nu\nu_L)|^2 + |\check{\mathcal{M}}_T(\tau \rightarrow \nu\nu_T)|^2 \right) D_v(m_v^2) g_v(m_v^2),$$

where  $D_v(m_v^2)$  is the Breit-Wigner with a running width,

$$D_v(m_v^2) = \left[ (m_v^2 - m_0^2)^2 + (m_v \Gamma_v)^2 \right]^{-1} \quad (50)$$

$$= \left[ (m_v^2 - m_0^2)^2 + (m_0 \Gamma_0)^2 \times \left( \frac{g_v(m_v^2)}{g_v(m_0^2)} \right)^2 \right]^{-1}. \quad (51)$$

For the  $\rho$ , we take  $m_0$  and  $\Gamma_0$  to be

$$m_{0,\rho} = 770 \text{ MeV}, \quad \Gamma_{0,\rho} = 150 \text{ MeV}.$$

For the  $a_1$ , we take  $m_0$  and  $\Gamma_0$  to be

$$m_{0,a} = 1.22 \text{ GeV}, \quad \Gamma_{0,a} = 420 \text{ MeV}.$$

For the decay  $\rho \rightarrow 2\pi$ , the simple chiral Lagrangian interaction

$$\mathcal{L}_{int} \propto \rho^\mu (\pi_1 \partial_\mu \pi_2 - \pi_2 \partial_\mu \pi_1)$$

suffices for our purposes and gives the line shape

$$g_\rho(m^2) = \text{const.} \times \frac{(m^2 - 4m_\pi^2)^{3/2}}{m}. \quad (52)$$

The parameterization of  $a_1$  decay, which proceeds dominantly through  $a_1 \rightarrow \rho\pi \rightarrow 3\pi$ , is more involved due to the multiple possible parameterizations of intermediate hadronic resonances in the chiral Lagrangian describing  $a_1$  dynamics. Again following [12], we use a parameterization of the running width  $g_a(m^2)$  due to [30],

$$g_a(m^2) = \begin{cases} 4.1(m^2 - 9m_\pi^2)^3 (1 - 3.3(m^2 - 9m_\pi^2) + 5.8(m^2 - 9m_\pi^2)^2) & m^2 < (m_\rho + m_\pi)^2 \\ m^2 \left( 1.623 + \frac{10.38}{m^2} - \frac{9.32}{m^4} + \frac{0.65}{m^6} \right) & m^2 \geq (m_\rho + m_\pi)^2 \end{cases} \quad (53)$$

All masses are in units of GeV. This particular parameterization follows from a model of  $a_1$  decay which goes through intermediate finite-width  $\rho$  alone, with no contribution from other resonances such as the radial excitations  $\rho', \rho''$ . The coefficients are obtained from a fit to experimental data [30].

Plugging in the matrix elements (49) for the initial decay  $\tau \rightarrow \nu v$  and doing some simplification, we have

$$d\Gamma \propto \int d\cos\theta dm_v^2 (m_\tau^2 - m_v^2)^2 \left[ 2 + \frac{m_\tau^2}{m_v^2} + \mathcal{P}_\tau \cos\theta \left( \frac{m_\tau^2}{m_v^2} - 2 \right) \right] D_v(m_v^2) g_v(m_v^2).$$

To change variables from  $\cos\theta$  to  $z$ , use (48), with  $m_v$  in place of  $m_\pi$ . With this substitution, we have

$$d\Gamma \propto \int_0^1 dz \int_{(nm_\pi)^2}^{zm_\tau^2} dm_v^2 \left[ \left( 1 - \frac{m_v^2}{m_\tau^2} \right) \left( 2 + \frac{m_\tau^2}{m_v^2} \right) + \mathcal{P}_\tau \left( (2z - 1) - \frac{m_v^2}{m_\tau^2} \right) \left( \frac{m_\tau^2}{m_v^2} - 2 \right) \right] \times D_v(m_v^2) g_v(m_v^2).$$

Finally then, we can write the contribution from the vector mesons as

$$\frac{1}{\Gamma} \frac{d\Gamma}{dz} = \text{const.} \times \int_{(nm_\pi)^2}^{zm_\tau^2} dm_v^2 \left[ \left( 1 - \frac{m_v^2}{m_\tau^2} \right) \left( 2 + \frac{m_\tau^2}{m_v^2} \right) + \mathcal{P}_\tau \left( (2z - 1) - \frac{m_v^2}{m_\tau^2} \right) \left( \frac{m_\tau^2}{m_v^2} - 2 \right) \right] \times D_v(m_v^2) g_v(m_v^2). \quad (54)$$

Using the lineshapes (52), (53) and carrying out the integral over  $m_v^2$  numerically gives the hadronic energy spectra  $P_{(\rho)}^\pm(z)$ ,  $P_{(a)}^\pm(z)$  which are plotted in Figure 17.

## Acknowledgments

We would like to thank Scott Thomas for collaboration and for many insightful conversations, as well as comments on the manuscript. We would also like to thank Amit Lath, Yifan Lin, Aneesh Manohar, Michael Peskin, and Steve Schnetzer for useful discussions. J.S. thanks the Kavli Institute for Theoretical Physics for hospitality. The work of M.G. was supported by Los Alamos National Laboratory. The work of J.S. was supported by DOE grant DE-FG02-96ER40959.

## References

- [1] S. Schael *et al.* [ALEPH Collaboration and DELPHI Collaboration and L3 Collaboration and OPAL Collaboration and LEP Working Group for Higgs Boson Searches], “Search for neutral MSSM Higgs bosons at LEP,” *Eur. Phys. J. C* **47**, 547 (2006) [arXiv:hep-ex/0602042].

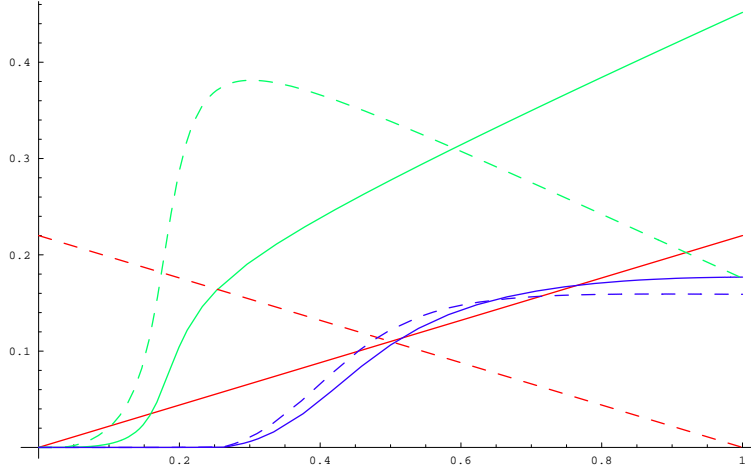


Figure 17: Contributions to the  $\tau$  daughter energy fraction distribution for hadronic one-prong taus, weighted by branching fraction. The three contributing decay modes are  $\tau \rightarrow \pi\nu$  (shown in red);  $\tau \rightarrow \rho\nu$  (shown in green) and  $\tau \rightarrow a_1\nu$  (shown in blue). Solid lines indicate the distributions for positive helicity tau, and dashed lines the contribution for negative helicity tau.

- [2] H. Baer, C. h. Chen, M. Drees, F. Paige and X. Tata, “Collider phenomenology for supersymmetry with large  $\tan(\beta)$ ” *Phys. Rev. Lett.* **79**, 986 (1997) [Erratum-ibid. **80**, 642 (1998)] [arXiv:hep-ph/9704457];
- [3] M. Perelstein and C. Spethmann, “A collider signature of the supersymmetric golden region ,” *JHEP* **0704**, 070 (2007) [arXiv:hep-ph/0702038].
- [4] M. Graesser, J. Shelton, and S. Thomas, “Discerning Supersymmetry in Cascade Decay Correlations,” to appear.
- [5] M. Burns, K. Kong, K. T. Matchev and M. Park, “A General Method for Model-Independent Measurements of Particle Spins, Couplings and Mixing Angles in Cascade Decays with Missing Energy at Hadron Colliders,” *JHEP* **0810**, 081 (2008) [arXiv:0808.2472 [hep-ph]].
- [6] A. J. Barr, “Using lepton charge asymmetry to investigate the spin of supersymmetric particles at the LHC,” *Phys. Lett. B* **596**, 205 (2004) [arXiv:hep-ph/0405052].
- [7] H. Baer, C. h. Chen, M. Drees, F. Paige and X. Tata, “Probing Minimal supergravity at the CERN LHC for large  $\tan(\beta)$  ,” *Phys. Rev. D* **59**, 055014 (1999) [arXiv:hep-ph/9809223]; I. Hinchliffe and F. E. Paige, “Measurements in SUGRA models with large  $\tan(\beta)$  at LHC,” *Phys. Rev. D* **61**, 095011 (2000) [arXiv:hep-ph/9907519].

- [8] G. L. Bayatian *et al.* [CMS Collaboration], “CMS technical design report, volume II: Physics performance,” Section 13.9.2, J. Phys. G **34**, 995 (2007); D. J. Mangeol, U. Goerlach, ”Search for  $\tilde{\chi}_2^0$  decays to  $\tilde{\tau}\tau$  and SUSY mass spectrum measurement using di- $\tau$  final states,” CMS Note 2006/096,
- [9] Y. S. Tsai, “Decay Correlations of Heavy Leptons in  $E^+ E^- \rightarrow \text{Lepton}^+ \text{Lepton}^-$ ” Phys. Rev. D **4**, 2821 (1971) [Erratum-ibid. D **13**, 771 (1976)].
- [10] K. Hagiwara, A. D. Martin and D. Zeppenfeld, “Tau Polarization Measurements at LEP and SLC,” Phys. Lett. B **235**, 198 (1990).
- [11] B. K. Bullock, K. Hagiwara and A. D. Martin, “Tau polarization as a signal of charged Higgs bosons,” Phys. Rev. Lett. **67**, 3055 (1991).
- [12] B. K. Bullock, K. Hagiwara and A. D. Martin, “Tau Polarization And Its Correlations As A Probe Of New Physics,” Nucl. Phys. B **395**, 499 (1993).
- [13] D. P. Roy, “Using tau polarization for the charged Higgs search at hadron colliders,” Phys. Lett. B **277**, 183 (1992).
- [14] B. K. Bullock, K. Hagiwara and A. D. Martin, “Tau Pair Polarization Correlations As A Signal For Higgs Bosons,” Phys. Lett. B **273**, 501 (1991).
- [15] G. L. Bayatian *et al.* [CMS Collaboration], “CMS technical design report, volume II: Physics performance,” Section 11.2.5, J. Phys. G **34**, 995 (2007); M. Baarmand, M. Hashemi, A. Nikitenko, ”Light Charged Higgs Discovery Potential of CMS in the  $H^\pm \rightarrow \tau\nu_\tau$  Decay with Single Lepton Trigger, CMS Note 2006/056.
- [16] M. M. Nojiri, “Polarization of tau lepton from scalar tau decay as a probe of neutralino mixing,” Phys. Rev. D **51**, 6281 (1995) [arXiv:hep-ph/9412374].
- [17] M. M. Nojiri, K. Fujii and T. Tsukamoto, “Confronting the minimal supersymmetric standard model with the study of scalar leptons at future linear  $e^+ e^-$  colliders,” Phys. Rev. D **54**, 6756 (1996) [arXiv:hep-ph/9606370].
- [18] S. Y. Choi, K. Hagiwara, Y. G. Kim, K. Mawatari and P. M. Zerwas, “Tau polarization in SUSY cascade decays,” Phys. Lett. B **648**, 207 (2007) [arXiv:hep-ph/0612237].
- [19] K. Mawatari, “Tau polarization in SUSY cascade decays at LHC,” arXiv:0710.4994 [hep-ph].

- [20] R. M. Godbole, M. Guchait and D. P. Roy, “Using Tau Polarization to probe the Stau Co-annihilation Region of mSUGRA Model at LHC,” arXiv:0807.2390 [hep-ph].
- [21] J. M. Smillie and B. R. Webber, “Distinguishing Spins in Supersymmetric and Universal Extra Dimension Models at the Large Hadron Collider,” JHEP **0510**, 069 (2005) [arXiv:hep-ph/0507170].
- [22] C. Athanasiou, C. G. Lester, J. M. Smillie and B. R. Webber, “Distinguishing spins in decay chains at the Large Hadron Collider,” JHEP **0608**, 055 (2006) [arXiv:hep-ph/0605286]; C. Athanasiou, C. G. Lester, J. M. Smillie and B. R. Webber, “Addendum to ‘Distinguishing spins in decay chains at the Large Hadron Collider’,” arXiv:hep-ph/0606212.
- [23] A. Alves, O. Eboli and T. Plehn, “It’s a gluino,” Phys. Rev. D **74**, 095010 (2006) [arXiv:hep-ph/0605067].
- [24] L. T. Wang and I. Yavin, “Spin Measurements in Cascade Decays at the LHC,” JHEP **0704**, 032 (2007) [arXiv:hep-ph/0605296].
- [25] T. Goto, K. Kawagoe and M. M. Nojiri, “Study of the slepton non-universality at the CERN Large Hadron Collider,” Phys. Rev. D **70**, 075016 (2004) [Erratum-ibid. D **71**, 059902 (2005)] [arXiv:hep-ph/0406317].
- [26] C. Amsler *et al.* [Particle Data Group], Phys. Lett. B **667**, 1 (2008).
- [27] Y. Lin and S. Schnetzer, *private communication*.
- [28] A. F. Falk and M. E. Peskin, “Production, decay, and polarization of excited heavy hadrons,” Phys. Rev. D **49**, 3320 (1994) [arXiv:hep-ph/9308241].
- [29] TAUOLA official homepage: <http://wasm.home.cern.ch/wasm/goodies.html>
- [30] J. H. Kuhn and A. Santamaria, “Tau decays to pions,” Z. Phys. C **48**, 445 (1990).